HHS Public Access

Author manuscript

Dev Cell. Author manuscript; available in PMC 2021 January 02.

Published in final edited form as:

Dev Cell. 2019 November 04; 51(3): 313–325.e10. doi:10.1016/j.devcel.2019.09.005.

The G2-to-M transition is ensured by a dual mechanism that protects cyclin B from degradation by Cdc20-activated APC/C

Pablo Lara-Gonzalez[1,2,*], **Mark W. Moyle**[1,2,3], **Jacqueline Budrewicz**[1,2], **Jose Mendoza-Lopez**[1,2], **Karen Oegema**[1,2], **Arshad Desai**[1,2,@,*]

[1]Ludwig Institute for Cancer Research, University of California San Diego, La Jolla, CA 92093, United States

[2]Department of Cellular & Molecular Medicine, University of California San Diego, La Jolla, CA 92093, United States

[3]Current address: Program in Cellular Neuroscience, Neurodegeneration, and Repair, Department of Cell Biology and Department of Neuroscience, Yale University School of Medicine, PO Box 9812, New Haven, CT 06536-0812, United States

SUMMARY

In the eukaryotic cell cycle, a threshold level of cyclin B accumulation triggers the G2-to-M transition and subsequent cyclin B destruction triggers mitotic exit. The Anaphase Promoting Complex/Cyclosome (APC/C) is the E3 ubiquitin ligase that, together with its co-activator Cdc20, targets cyclin B for destruction during mitotic exit. Here we show that two pathways act in concert to protect cyclin B from Cdc20-activated APC/C in G2, in order to enable cyclin B accumulation and the G2-to-M transition. The first pathway involves the Mad1-Mad2 spindle checkpoint complex, acting in a distinct manner from checkpoint signaling after mitotic entry but employing a common molecular mechanism–the promotion of Mad2-Cdc20 complex formation. The second pathway involves cyclin-dependent kinase phosphorylation of Cdc20, which is known to reduce Cdc20's affinity for the APC/C. Cooperation of these two mechanisms, which target distinct APC/C binding interfaces of Cdc20, enables cyclin B accumulation and the G2-to-M transition.

Graphical Abstract

[*]Corresponding authors: abdesai@ucsd.edu (A.D.); plgonzalez@ucsd.edu (P.L.-G.).

AUTHOR CONTRIBUTIONS

P.L-G., M.W.M. and A.D. initiated the project; P.L-G. performed the majority of experiments with help from J.B. and J.M-L.; K.O. and A.D. supervised the project and P.L-G., K.O. and A.D. prepared the manuscript, with input from other authors.

[@]:Lead contact

DECLARATION OF INTERESTS:

Authors declare no competing interests.

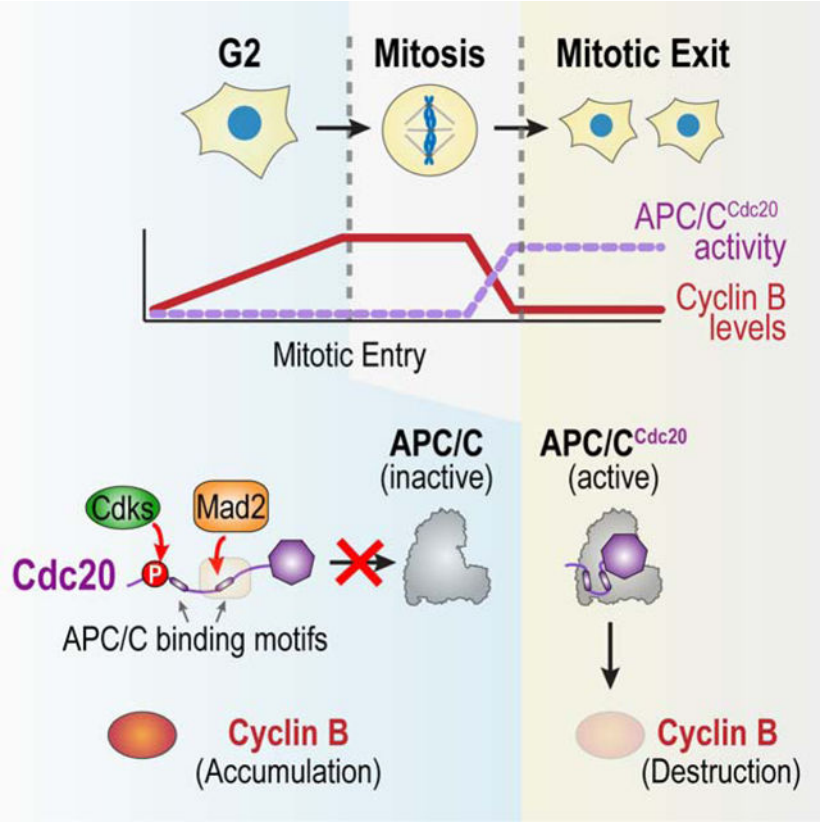

eTOC Blurb

Lara-Gonzalez *et al.* show that the spindle checkpoint protein Mad2 acts in concert with cyclin-dependent kinase phosphorylation to promote the G2-to-M transition in the cell cycle. The two mechanisms act in parallel to suppress the cyclin degradation machinery in G2, thereby allowing cyclin B accumulation and transition into M phase.

Keywords

Mitosis; cell division; germline; spindle checkpoint; Mad2; Mad1; APC/C; Cdc20; Cdk1; cyclin B3

INTRODUCTION

The rise and decay in Cdk1-cyclin B activity drives eukaryotic cells into and out of M phase in the cell cycle (Morgan, 2007; Ferrell, 2013). While Cdk1 protein levels are relatively constant during the cell cycle, cyclin B periodically accumulates until it reaches a critical threshold that, through a series of feedback mechanisms, leads to high Cdk1-cyclin B kinase activity (Morgan, 2007; Ferrell, 2013). High Cdk1-cyclin B kinase activity drives striking cellular changes associated with mitosis—genome compaction, nuclear envelope breakdown, centrosome separation, bipolar spindle formation, and assembly of kinetochores that couple chromosomes to spindle microtubules (Morgan, 2007). Once all chromosomes have attached to spindle microtubules, cyclin B degradation is initiated to drive mitotic exit.

The APC/C is the multi-subunit E3 ubiquitin ligase that, when bound to its co-activator Cdc20, targets cyclin B as well as securin, an inhibitor of sister chromatid separation, for proteolytic degradation (Peters, 2006; Pines, 2011; Alfieri et al., 2017).

To achieve the periodic accumulation and decline of cyclin B levels that demarcates M phase in the cell cycle, APC/C^{Cdc20} must be restrained to enable sufficient cyclin B accumulation to trigger the G2-to-M transition (Lara-Gonzalez et al., 2017). Once mitosis is initiated, APC/C^{Cdc20} must also be restrained until all chromosomes are connected to the spindle, in order to prevent errors in chromosome segregation. Recent work has greatly advanced our understanding of how unattached chromosomes inhibit APC/C^{Cdc20} during mitosis, via the spindle checkpoint pathway that is activated at kinetochores (Musacchio, 2015; Corbett, 2017). The kinetochore-based spindle checkpoint produces a diffusible inhibitor of the APC/C^{Cdc20}, known as the mitotic checkpoint complex. A central component of the mitotic checkpoint complex is the protein Mad2, which exists in two conformations: open and closed (Luo et al., 2002; Sironi et al., 2002). The closed form of Mad2 is bound to related peptide motifs from its cellular partners, Mad1 and Cdc20. When the spindle checkpoint is active, Mad1-Mad2 complexes concentrate at unattached kinetochores where they recruit soluble open Mad2 and catalyzes its conversion to form a closed complex with Cdc20. Kinetochore-generated Mad2-Cdc20 complex then associates with Mad3 (known as BubR1 in vertebrates)–Bub3 to generate the mitotic checkpoint complex (Musacchio, 2015; Corbett, 2017). The mitotic checkpoint complex is a potent inhibitor of already-active APC/C^{Cdc20} that acts by binding to the APC/C^{Cdc20} holocomplex and interfering with its ability to recruit E2 ubiquitin-conjugating enzymes and to recognize substrates (Izawa and Pines, 2015; Alfieri et al., 2016; Yamaguchi et al., 2016). Early in mitosis, prior to assembly of mature kinetochores, Mad1-Mad2 complex localized at nuclear pores is proposed to generate the mitotic checkpoint complex via a similar reaction (Rodriguez-Bravo et al., 2014).

In contrast to APC/C^{Cdc20} regulation by kinetochores in mitosis, how APC/C^{Cdc20} is restrained during G2 to allow cyclin B accumulation and the G2-to-M transition is not understood. The APC/C inhibitor Emi1 was initially proposed to block APC/C^{Cdc20} activity in G2 (Reimann et al., 2001). However, subsequent work showed that Emi1 targets APC/C bound by its other co-activator, Cdh1, and its primary function is to prevent re-replication of DNA (Di Fiore and Pines, 2007; Machida and Dutta, 2007). Emi2, related to Emi1, was shown to inhibit APC/C^{Cdc20} during oocyte meiotic arrest (Schmidt et al., 2005; Tung et al., 2005); however, knockout analysis has shown that Emi2 is dispensable for somatic divisions in mammals (Gopinathan et al., 2017). In addition, Emi proteins are not as widely conserved as cyclin B and the APC/C. Other mechanisms suggested to restrain APC/C^{Cdc20} include the N-terminal region of BubR1(Mad3) (Malureanu et al., 2009), phosphorylation of Cdc20 by cyclin-dependent kinases (Hein and Nilsson, 2016), and requirement for phosphorylation of core APC/C subunits by the mitotic kinases Cdk1 and Plk1 to promote Cdc20 binding (Fujimitsu et al., 2016; Qiao et al., 2016; Zhang et al., 2016). The last idea has strong support from biochemical, structural and *Xenopus* egg extract studies—egg extracts rapidly cycle between S and M phases without an intervening G2 phase—but its importance in wider cellular contexts has not been assessed. Thus, in contrast to the mechanistic understanding of how active APC/C^{Cdc20} is regulated by the spindle checkpoint after mitotic

entry, there is less clarity on how APC/C^{Cdc20} is restrained to allow sufficient cyclin B accumulation for the G2-to-M transition.

Here, by analyzing proliferation in the *C. elegans* germline, and supporting key findings in human cultured cells, we define two parallel-acting mechanisms that target Cdc20 to suppress APC/C^{Cdc20} activation and enable the G2-to-M transition. The first mechanism involves the Mad1-Mad2 complex acting in a manner distinct from its well-defined spindle checkpoint function that requires kinetochore localization. The second mechanism involves phosphorylation of Cdc20 that reduces its binding affinity for the APC/C. Inhibition of both mechanisms disrupts the G2-to-M transition to a similar extent as inhibition of core mitotic entry circuit factors, such as Cdk1 and cyclin B. In addition to identifying a dual inhibitory mechanism that restrains APC/C^{Cdc20} to enable the G2-to-M transition, these results reveal a conserved checkpoint signaling-independent function of the Mad1-Mad2 complex.

RESULTS

Mad2 has a spindle checkpoint-independent function that is essential for viability and fertility in *C. elegans*

When the spindle checkpoint is activated, unattached kinetochores catalyze formation of the mitotic checkpoint complex, containing Mad2 and Mad3(BubR1) that binds to and inhibits Cdc20-activated APC/C (Musacchio, 2015; Corbett, 2017) (Fig. 1A). We confirmed equal importance of MAD-2 and MAD-3 for spindle checkpoint signaling in *C. elegans* by generating deletions of *mad-2* and *mad-3* using CRISPR/Cas9 (Figs. S1A,B), and characterizing null mutant embryos using a checkpoint assay that overcomes the drug impermeability of *C. elegans* embryos (Essex et al., 2009; Kim et al., 2017). In this assay, monopolar spindles with unattached kinetochores are generated during the second embryonic division by inhibition of a protein required for centriole duplication (Figs. 1B,C). Spindle checkpoint activation at the unattached kinetochores extends mitotic duration ~6–7 fold (Figs. 1B,C) (Kim et al., 2017); this extension was not observed in embryos lacking either MAD-2 or MAD-3 (Figs. 1B,C). (Movie S1).

Despite their equivalent requirement for checkpoint signaling, the phenotypes observed in *mad-2Δ* and *mad-3Δ* worms were strikingly different. While *mad-2Δ* progeny of heterozygous mothers developed into adults, they exhibited significantly lower fertility and embryonic viability compared to *mad-3Δ* worms; after three generations, *mad-2Δ* worms produced a few, mostly dead, embryos (Fig. 1D). By contrast, *mad-3Δ* worms laid a constant number of progeny that was ~2/3 of that in control worms. Numerous developmental abnormalities were observed for *mad-2Δ* but not *mad-3Δ* animals (Fig. S1C), consistent with prior analysis of *mad-2* and *mad-3* mutants that partially deleted their coding regions (Kitagawa and Rose, 1999; Stein et al., 2007) and with RNAi-mediated depletion of MAD-2 and MAD-3 (Figs. S1D–F). These observations indicate that MAD-2 has a checkpoint signaling-independent role in fertility and viability.

Serendipitous support for the conclusion that MAD-2 has a checkpoint-independent function came from *in situ* tagging of MAD-2 and its binding partner MAD-1 with GFP (Figs. 1E; S1G). *In situ* GFP-tagged MAD-1 localized to kinetochores and supported checkpoint

signaling, fertility, and embryonic viability. By contrast, the MAD-2::GFP fusion failed to localize to kinetochores and was inactive in checkpoint signaling (Figs. 1E,F), but nonetheless exhibited fertility and embryonic viability similar to *mad-3*Δ worms (Fig. 1G). These results suggest that *mad-2::gfp* is a separation-of-function allele that supports fertility and viability but not spindle checkpoint signaling. They also suggest that the role of MAD-2 in fertility and embryonic viability does not require its localization to kinetochores.

Mad2 is a conserved regulator of the G2-to-M transition

The most prominent phenotype of *mad-2Δ* worms was an abrupt reduction in fertility, suggesting that MAD-2 is important for germline development. To analyze the effect of MAD-2 and MAD-3 inhibition on germline development, we used an assay in which the introduction of food triggers germ cell proliferation in larvae (Fig. S2A). In *C. elegans*, the germline arises from a pair of progenitor cells that are quiescent in G2 phase of the cell cycle (Fukuyama et al., 2006). Feeding at the L1 larval stage triggers proliferation of these progenitors, producing nascent germlines with 20–30 cells within 20h (Fig. 2A).

Depletion of MAD-2 or MAD-3 did not affect germ cell quiescence in larvae held for up to 4 days in the absence of food (*not shown*). By contrast, MAD-2 depletion led to a significant reduction in the rate of germ cell proliferation, whereas MAD-3 depletion had no effect (Fig. 2A); similar results were obtained using mutants instead of RNAi (Fig. S2B). Exponential fits revealed that MAD-2 depletion increased germ cell doubling time by ~50%, from 4.7h to 6.9h. Thus MAD-2 has a checkpoint signaling-independent function in germ cell proliferation.

Germ cells have a negligible G1 phase and initiate S-phase immediately after nuclei reform in telophase (Fig. S2C; Movie S2) (Fox et al., 2011; Seidel and Kimble, 2015). To determine which cell cycle phase (S, G2 or M) was affected by MAD-2 depletion, we imaged GFP-tagged $PCNA^{PCN-1}$, which concentrates in replication foci during S-phase but is diffuse in G2 nuclei (Fig. 2B). In control larvae, ~60% of germ cells were in S-phase, and ~40% were in G2; only a minor percentage (3.5%) were in M-phase (Fig. S2D; (Fox et al., 2011)). In *mad-2(RNAi)* larvae, the proportions were reversed with ~40% of germ cells in S-phase and ~60% in G2 (Figs. 2B; S2D). Combining these numbers with the doubling time measurements indicated that in *mad-2(RNAi)* the duration of S phase was unchanged whereas G2 duration more than doubled (Fig. 2C). Thus, MAD-2 promotes the G2-to-M transition. In support of this conclusion, a similar phenotype was observed for a temperature-sensitive mutant of CDK-1 (*cdk-1(ne2257)* (Shirayama et al., 2006) (Figs. 2D; S2E).

To determine if the role of Mad2 in promoting the G2-to-M transition is conserved, we analyzed human U2OS cells expressing fluorescent PCNA and histone H2b; the interval between dissolution of PCNA foci and nuclear envelope breakdown (NEBD) provides a measure for the G2-to-M transition in individual cells (Leonhardt et al., 2000; de Groot et al., 2015) (Fig. 2E). Depletion of Mad2, but not BubR1, the human Mad3 homolog, significantly delayed the G2-to-M transition (Figs. 2F; S2F; Movie S3), while both depletions abolished spindle checkpoint signaling (Fig. S2G). The delay caused by Mad2 depletion was suppressed by expression of siRNA-resistant Myc-Mad2, indicating that it is

not due to an off-target effect (Fig. S2H–I). Thus, Mad2 has a conserved role in promoting the G2-to-M transition and this function is distinct from its role in the spindle checkpoint after mitotic entry. Notably, MAD-2 depletion did not affect cell cycle progression during rapid embryonic divisions in *C. elegans* that cycle between S and M phases (*not shown*), suggesting that it acts in cell cycles with a defined G2 phase.

Mad2 acts in the cytoplasm in a complex with Mad1 to promote the G2-to-M transition

To determine how Mad2 promotes the G2-to-M transition, we focused on *C. elegans* germ cells, where loss of the checkpoint function of Mad2 has a relatively minor effect. Mad2 is present in a 2:2 hetero-tetrameric complex with Mad1 and in a free monomeric pool (Chung and Chen, 2002; Sironi et al., 2002; Shah et al., 2004; De Antoni et al., 2005) (Fig. 3A). In addition to localizing to unattached kinetochores in mitosis, the Mad1-Mad2 complex localizes in interphase to nuclear pores, through a direct interaction of Mad1 with the nuclear pore basket component Tpr (NPP-21 in *C. elegans*) (Chen et al., 1998; Campbell et al., 2001; Lee et al., 2008), and to the nucleoplasm, via a nuclear localization sequence (NLS) in Mad1 (Scott et al., 2005).

To determine if complex formation between MAD-2 and MAD-1 is required for promoting the G2-to-M transition, we replaced endogenous MAD-1 with a mutant that disrupts the MAD-2 interaction motif (MIM; Fig. 3B; S3A) (Luo et al., 2002; Sironi et al., 2002)). MAD-1 MIM^{Mut} localized to unattached kinetochores and to the nuclear periphery similarly to wild-type (WT) MAD-1 (Figs. S3B,C) but was defective in spindle checkpoint signaling (Fig. S3D). Notably, MAD-1 MIM^{Mut} reduced the rate of germ cell proliferation (Fig. 3C) and compromised fertility (Fig. S3E) to a similar extent as *mad-2Δ* (Fig. 1D). By contrast, replacing MAD-1 with a mutant that cannot bind Tpr and lacked the NLS (MAD-1 Tpr^{mut} & NLS^{mut}), and therefore failed to localize to the nuclear periphery or interior (Figs. 3D; S3F–I), did not affect the rate of germ cell proliferation (Figs. 3E; S3J). Thus, MAD-2 must interact with MAD-1 to promote the G2-to-M transition and this function can be executed in the cytoplasm.

Mad2 interacts with Cdc20 in order to promote the G2-to-M transition

The Mad1–Mad2 complex interacts with free Mad2 and converts it from an open to a closed conformation that forms a complex with Cdc20 (Fig. 3A) (De Antoni et al., 2005). To test if MAD-2 association with CDC-20, which is expressed in the cytoplasm of germ cells (Fig. S4A), is important for promoting the G2-to-M transition, we engineered a CDC-20 mutant (CDC-20 ΔPPP) that specifically compromised its ability to bind to MAD-2 (Hwang et al., 1998) (Fig. 3F). Replacing endogenous CDC-20 with CDC-20 ΔPPP mutant abrogated spindle checkpoint signaling without affecting normal mitotic duration, indicating that CDC-20 ΔPPP retained the ability to normally activate the APC/C (Figs. 3G; S4B,C). CDC-20 ΔPPP reduced the rate of germ cell proliferation and caused a fertility defect that mimicked *mad-2* loss (Figs. 3H; S4D). By contrast, a different CDC-20 mutant (CDC-20 A138V; Stein et al., 2007; Kim et al., 2017) that disrupts spindle checkpoint signaling but maintains the ability to interact with MAD-2, did not affect the rate of germ cell proliferation (Figs. 3F–H; S4B–D). Thus, the ability of MAD-2 to promote the G2-to-M transition requires MAD-2 to bind to CDC-20.

The ability of the Mad1-Mad2 complex to catalyze the conformational change in Mad2 that promotes Mad2-Cdc20 complex formation involves dimerization of free Mad2 with Mad1-bound (Fig. 3A; (De Antoni et al., 2005)). When expressed in the absence of endogenous MAD-2, a mutant version of MAD-2 that cannot dimerize (the MAD-2 R133E; Q134A mutant, De Antoni et al., 2005) resulted in severe fertility and viability defects (Figs. S4E–H). Thus, a MAD-1–MAD-2 template-mediated formation of a MAD-2–CDC-20 complex is important for a normal G2-to-M transition.

The Mad1-Mad2 complex promotes the G2-to-M transition by inhibiting APC/C^{Cdc20}

MAD-2 binding to CDC-20 interferes with an APC/C binding region in CDC-20 called the KILR motif (Tang et al., 2001; Fang, 2002; Izawa and Pines, 2012) (Fig. 3F). This fact suggests that MAD-1–MAD-2 promotes the G2-to-M transition by preventing CDC-20 from associating with and activating the APC/C. A prediction of this model is that reducing APC/C activity should alleviate the effect of MAD-2 inhibition on the G2-to-M transition.

To test this prediction, we analyzed temperature-sensitive mutants in two different APC/C subunits, *Apc8*^{ts} (*mat-3(or344)*) (Rappleye et al., 2002) and *Apc6*^{ts} (*emb-37(g48)*) (Golden et al., 2000) (Fig. 4A), as well as a mutant of CDC-20 in its WD40 domain, D433N, which reduces APC/C^{CDC-20} activity (Kitagawa et al., 2002). Compromised APC/C function in all 3 mutants was evident from prolonged mitotic duration in one-cell embryos (Fig. 4A). All 3 mutants suppressed the germ cell proliferation defect resulting from MAD-2 depletion (Fig. 4B); the *Apc8*^{ts} and *Apc6*^{ts} mutants also partially suppressed the *mad-2Δ* fertility defect (Fig. S5A). Thus, the MAD-1–MAD-2 complex promotes the G2-to-M transition by catalyzing formation of a MAD-2–CDC-20 complex and suppressing APC/C activity, likely by sequestering CDC-20 to limit formation of active APC/C^{CDC-20} complexes.

Mad1-Mad2 protects Cyclin B during its accumulation in G2

To determine if MAD-1–MAD-2 promoted the G2-to-M transition by protecting cyclin B from APC/C^{Cdc20}-mediated degradation during G2, we first identified the cyclin B isoform that promotes mitotic entry in *C. elegans* germ cells. *C. elegans* has 3 cyclin Bs: cyclin B1 (CYB-1), cyclin B2 (CYB-2, encoded by two closely related genes *cyb-2.1* and *cyb-2.2*) and cyclin B3 (CYB-3) (Kreutzer et al., 1995; van der Voet et al., 2009). Inhibition of CYB-3, but not of CYB-1 and CYB-2, mimicked loss of CDK-1 (Fig. 4C), indicating that CYB-3 is the dominant cyclin B required for mitotic entry in the germline (Green et al., 2011; Yoon et al., 2012).

The sensitivity of germ cell divisions to larval immobilization methods necessary for live imaging precluded quantitative comparison of CYB-3 accumulation in control and MAD-2-depletions. Therefore, as an alternative approach, we tested if providing extra CYB-3 bypassed the need for MAD-1–MAD-2. A single copy transgene expressing CYB-3, under control of endogenous regulatory elements (Fig. S5C), rescued the lethality of a *cyb-3* null mutant (Figs. S5D,E). When introduced into a wildtype background, the extra CYB-3 suppressed the germ cell proliferation defect of *mad-2(RNAi)* (Fig. 4D); extra CYB-3 also partially suppressed the fertility defect of *mad-2Δ* (Fig. S5F). By contrast, extra CYB-1 had

no effect (Figs. 4D; S5C–F). These data are consistent with duplication of *cyb-3* acting as a weak suppressor of *mad-1Δ* (Tarailo-Graovac et al., 2010).

In contrast to germ cells in motile *C. elegans* larvae, live imaging of cyclin B is feasible in human cells (Clute and Pines, 1999). In U2OS cells, we *in situ*-tagged cyclin B1 (encoded by *CCNB1*), the cyclin B isoform essential for mitotic entry in mammals, with mNeongreen (mNG) (Figs. 4E; S5G,H). In control cells, Cyclin B1-mNG steadily accumulated until NEBD and then declined as cells exited mitosis (Figs. 4F,G; Movie S4). The rate of cyclin B1 accumulation was significantly reduced in Mad2-depleted cells, which entered mitosis with ~70% of cyclin B1 levels at NEBD in control cells (Figs. 4F,G; Movie S4). These observations are reminiscent of a previous report that used Mad1 knockout RPE-1 cells (Rodriguez-Bravo et al., 2014). By contrast, depletion of BubR1 had no significant effect on cyclin B1 accumulation prior to NEBD, even though both BubR1 and Mad2 depletions resulted in equivalently rapid and premature degradation of cyclin B1 after mitotic entry (Figs. 4F,G; Movie S4). Collectively, the analysis in *C. elegans* germ cells and in human cells indicates that Mad1–Mad2 suppress APC/C^{Cdc20} activity in order to protect cyclin B during its accumulation prior to the G2-to-M transition.

Cyclin-dependent kinase phosphorylation of Cdc20 acts in parallel to Mad1-Mad2 to enable the G2-to-M transition

The above data show that, while the Mad1-Mad2 complex plays a conserved role in promoting the G2-to-M transition, its inhibition delays but does not block mitotic entry. This observation suggested that there is an additional mechanism that helps restrain APC/C^{Cdc20} in G2. Cdc20 phosphorylation by Cdk1/2 is one such potential mechanism, as phosphorylation reduces the binding affinity of Cdc20 for the APC/C (Fig. 5A) (Yudkovsky et al., 2000; Labit et al., 2012; Hein and Nilsson, 2016; Kim et al., 2017). The Cdk phosphorylation sites in Cdc20 are conserved and are located near the C-box, a key APC/C binding motif (Labit et al., 2012). In prior work we showed that CDC-20 was phosphorylated at three conserved sites in *C. elegans*, and that replacement of CDC-20 with a mutant (3A) that prevents phosphorylation significantly accelerated APC/C activation after NEBD in the early embryo (Kim et al., 2017).

To determine if Cdc20 phosphorylation acts in concert with Mad1–Mad2 to restrain APC/C activity in G2, we used *C. elegans* strains in which the sole source of CDC-20 was the non-phosphorylatable 3A mutant (Kim et al., 2017). To avoid the synthetic lethality that is observed when CDC-20 3A is combined with spindle checkpoint inhibition in embryos (Kim et al., 2017), we subjected L1 larvae to a post-hatching RNAi protocol that results in partial MAD-2 inhibition. Loss of CDC-20 phosphorylation or partial MAD-2 inhibition did not significantly affect germline development; however, combining the two perturbations led to a near-complete blockade of germ cell proliferation and was associated with a significant increase in nuclear size (Figs. 5B; S6A). Analysis of later larval stage germlines showed that combining CDC-20 3A with partial MAD-2 depletion resulted in a defect that was comparable to inhibition of essential mitotic entry factors such as CDC-25, CDK-1 and CYB-3 (Figs. 5C; S6B). A characteristic feature of this phenotype is giant nuclei, which likely arise from endoreduplication after failed mitotic entry (Figs. 5C; S6B) (Edgar and

Orr-Weaver, 2001; Green et al., 2011). Analysis using the GFP::PCNA^{PCN-1} reporter indicated that the combined inhibition resulted in a high proportion of cells arrested in G2 (Fig. 5D). As expected based on MAD-3 not being required to promote the G2-to-M transition, MAD-3 inhibition did not synergize with loss of CDC-20 phosphorylation (Fig. S6C).

The next question we addressed was which cyclin-Cdk complex targets CDC-20 to promote the G2-to-M transition in germ cells. CYB-3–CDK-1 could promote its own accumulation by phosphorylating CDC-20 as part of a feedback loop or a different cyclin-Cdk complex could be responsible for CDC-20 phosphorylation. An attractive candidate for the cyclin in the kinase complex targeting CDC-20 in germ cells is CYB-1, which is expressed in germ cells (Fig. S6D) but whose inhibition has little effect on germ cell proliferation (Figs. 4C; S6E). In support of this idea, CYB-1 inhibition phenocopied the CDC-20 3A mutant when combined with partial MAD-2 inhibition (Fig. S6E).

Cdc20 removal and replacement is challenging in human cells, with depletion sufficient to block APC/C activation being difficult to achieve (Wolthuis et al., 2008). We therefore tested if partial Cdk1 inhibition synergized with Mad2 depletion, using the small molecule inhibitor RO-3306 (Vassilev et al., 2006) (Fig. 5E). Monitoring the G2-to-M transition in single cells (Fig. 2E), we found that 5 μM RO-3306 delayed entry into mitosis and caused a small fraction (~15%) of cells that dissolved PCNA foci not entering mitosis during the filming session. The effect of RO-3306 was significantly enhanced by Mad2 depletion, with ~40% of cells not entering mitosis and the remainder exhibiting a much greater delay than RO-3306 treatment alone (Fig. 5E). While this result does not directly implicate Cdc20 regulation by Cdk1 in human cells, it supports the notion that Mad2 acts in parallel with a Cdk1 activity-dependent mechanism to promote the G2-to-M transition.

DISCUSSION

The results shown here highlight two distinct mechanisms that target Cdc20 and act in concert to enable cyclin B accumulation and promote the G2-to-M transition. The first mechanism involves the Mad1-Mad2 complex and the second phosphorylation of Cdc20 by cyclin-dependent kinases (Fig. 6A). The findings lead to a model in which Cdc20 phosphorylation and Mad2 binding cooperatively reduce affinity of Cdc20 for the APC/C in G2 by targeting two conserved regions, the C-box and the KILR motif, that are employed by Cdc20 to bind to distinct parts of the Apc8B subunit of the APC/C (Fig. 6B) (Zhang et al., 2016). Mad2 binds adjacent to and sterically blocks the KILR motif whereas Cdc20 phosphorylation electrostatically inhibits interaction of the C-box with Apc8B (Izawa and Pines, 2012; Labit et al., 2012). This coordinated action prevents formation of active APC/C^{Cdc20} complexes, thereby protecting cyclin B during its synthesis and enabling the G2-to-M transition. These findings illuminate a poorly understood feature of the eukaryotic cell cycle and identify a new conserved function for a central component of the spindle checkpoint pathway.

Distinct roles for Mad1-Mad2 in mitotic entry and in the spindle checkpoint

Using *C. elegans* and human cultured cells, we show that Mad1-Mad2 promotes mitotic entry by restricting the ability of APC/C^{Cdc20} to target cyclin B for degradation. The Mad1-Mad2 reaction that promotes mitotic entry has different requirements from the Mad1-Mad2-based spindle checkpoint pathway. Mad1-Mad2 function in the spindle checkpoint requires docking onto kinetochores and/or nuclear pores, where kinase activities catalyze the formation of a Mad2-Cdc20 complex that associates with Mad3(BubR1)-Bub3 to produce the mitotic checkpoint complex, a potent inhibitor of already-active APC/C^{Cdc20} (Musacchio, 2015; Corbett, 2017). In contrast, we show that the of Mad1-Mad2 in promoting the G2-to-M transition does not require kinetochore/nuclear pore docking or formation of the mitotic checkpoint complex and most likely acts by sequestering Cdc20 from forming active holocomplexes with the core APC/C (Fig. 6B).

Our data do not support the idea that an interphase form of the mitotic checkpoint complex is needed to inhibit APC/C^{Cdc20} prior to the G2-to-M transition (Rodriguez-Bravo et al., 2014). This is evident from imaging of *in situ*-tagged cyclin B1 in human cells, where cyclin B1 levels prior to NEBD were similar between control and BubR1 depletion, even though cyclin B1 was immediately degraded following mitotic entry in the latter (Fig. 4G). Our findings also challenge a prior study where the N-terminus of BubR1, but not Mad2, was suggested to control cyclin B accumulation during mitotic entry in mouse embryonic fibroblasts (Malureanu et al., 2009); while the precise reasons for the difference will require future independent efforts to clarify, our results are supported by analysis in the highly divergent contexts of *C. elegans* germ cells and human cultured cells; in addition, we employed *in situ*-tagged cyclin B, in contrast to transfected cyclin B fusions in the prior study, which enabled rigorous comparison between different perturbations. While MCC containing BubR1 does exist at low levels prior to mitosis (e.g. Kim et al., 2018), we speculate that in interphase, where the affinity of Cdc20 for the APC/C is low, Mad2 is sufficient to sequester Cdc20, whereas the high affinity of Cdc20 for the APC/C in mitosis due to APC/C phosphorylation (*see below*) requires the full MCC to efficiently inhibit active APC/C^{Cdc20}.

In the spindle checkpoint, concentration of Mad1-Mad2 in the vicinity of kinase activities at the kinetochore accelerates the conformational transition of free Mad2 promoted by the Mad1-Mad2 complex (Kulukian et al., 2009; Faesen et al., 2017). Our results suggest that, prior to mitotic entry, Mad1-Mad2 complexes are acting in the cytoplasm to promote a similar association of free Mad2 with Cdc20. Inhibition of Mps1, the kinase activating Mad1-Mad2 in human cells at the kinetochore, does not affect the G2-to-M transition (R. Kabeche & A. Desai, unpublished data). Thus, either a different kinase activity is involved or the basal uncatalyzed rate of Mad2's conformational transition by Mad1-Mad2 is sufficient to promote the G2-to-M transition. It will be important to elucidate in future work if and how the Mad1-Mad2 complex is regulated to promote the G2-to-M transition.

Direct targeting of Cdc20 is likely essential for the G2-to-M transition in cells with a defined G2 phase

In addition to Mad1-Mad2 catalyzed Mad2/Cdc20 complex formation, Cdc20 phosphorylation by Cdks, which reduces the affinity of its C-box-mediated interaction with the Apc8B subunit of the APC/C (Labit et al., 2012), is important to prevent APC/C activation prior to mitotic entry. Our data in *C. elegans* germ cells highlight the existence of a regulatory relay mechanism, in which a Cdk1-cyclin B1 complex phosphorylates Cdc20 to promote accumulation of cyclin B3, which is the major Cdk1 activator for mitotic entry in this tissue. In mammalian cells, where mitotic entry is driven by cyclin B1, cyclin A2-Cdk2, active in late S and G2 phases, has been proposed to be the kinase complex that phosphorylates Cdc20 (Hein and Nilsson, 2016), suggesting the existence of a conceptually similar relay mechanism. The severity of the defect in the G2-to-M transition when both Mad1–Mad2 and Cdc20 phosphorylation are simultaneously inhibited highlights the importance of keeping Cdc20 from activating the APC/C in order to enable entry into mitosis.

Recent work has identified a different mechanism that controls APC/C^{Cdc20} activity that is intrinsic to the APC/C (Morgan, 2016). In this mechanism, a loop region of Apc1 limits binding of the C-box of Cdc20 until Cdk activity-dependent phosphorylation causes loop displacement (Fujimitsu et al., 2016; Qiao et al., 2016; Zhang et al., 2016). Our work suggests that, while this mechanism is likely sufficient for coupling APC/C^{Cdc20} activation to Cdk activity in rapid embryonic divisions that alternate between S and M phases, it does not restrain APC/C^{Cdc20} activation to a sufficient extent to enable the G2-to-M transition in *C. elegans* germ cells and human somatic cells that have a defined G2 phase. We speculate that an additional level of control is required in cells with a G2 phase because of Cdk-cyclin activity that is present, e.g. cyclin A2-Cdk2 in human cells (Yam et al., 2002) and cyclin B1-Cdk1 in *C. elegans* germ cells (Figs. S6D,E), that relieves the APC/C-intrinsic autoinhibition mechanism. Thus, to enable cyclin B accumulation in G2, it becomes essential to prevent Cdc20 from binding to the APC/C. In rapid embryonic cycles, Cdk activity (comprised of Cdk1-cyclin B) is only prominent in M-phase, thereby making the APC/C-intrinsic mechanism sufficient. Integration of the two mechanisms we describe here with genetic perturbation of the Cdk-mediated relief of APC/C autoinhibition will be an important future goal.

Our work does not address how APC/C activated by its other co-activator, Cdh1/Hct1/Fizzy-related (Schwab et al., 1997; Visintin et al., 1997), is suppressed during mitotic entry. As Mad2 does not bind to Cdh1, it is unlikely to directly control APC/C^{Cdh1} activity. Emi1 and Cdk phosphorylation have both been suggested to inhibit APC/C^{Cdh1} (Zachariae et al., 1998; Jaspersen et al., 1999; Grosskortenhaus and Sprenger, 2002). Notably, Emi1 inhibition of APC/C^{Cdh1} is important to prevent re-replication (Di Fiore and Pines, 2007; Machida and Dutta, 2007), highlighting that APC/C^{Cdh1} is suppressed during S and G2 phases. However, Emi1 is not conserved in species like *C. elegans*, suggesting that Cdk phosphorylation is also a potentially conserved mechanism suppressing APC/C^{Cdh1}, a possibility that will need to be addressed in future work.

In summary, we establish here the existence of two distinct mechanisms acting on Cdc20 to protect cyclin B during its accumulation and thereby enable the G2-to-M transition in the eukaryotic cell cycle. The fact that cells can still enter mitosis following loss of either mechanism and that these mechanisms likely do not operate in rapid embryonic divisions lacking a G2 phase, explains why they were not appreciated in prior efforts. Notably, one of the mechanisms we uncover involves a core spindle checkpoint complex acting outside of the context of chromosome segregation during mitosis. The mechanisms we describe are likely to broadly control cell division cycles with a defined G2 phase, during which genome integrity is ensured prior to commitment to mitosis.

STAR METHODS

Contact For Reagent And Resource Sharing

Further information and requests for resources and reagents should be directed to and will be fulfilled by the Lead Contact, Arshad Desai (abdesai@ucsd.edu).

Experimental Model And Subject Details

C. elegans* strains—C. elegans* strains were maintained in nematode growth media (NGM) plates seeded with the *Escherichia coli* OP50 strain at 20°C, with the exception of tempera ture-sensitive mutant for *cdk-1* (*cdk-1(ne2257)*) that was maintained at 16°C. The list of strains used in this study is in the Key Resources Table.

Cell lines—U2OS cells were maintained in McCoy's 5A (Modified) Medium (Gibco), supplemented with 10% Fetal Bovine Serum in a humidified incubator at 37°C with 5% CO2.

Method Details

Generation of transgenic *C. elegans* strains—Transgenes were inserted at a single locus in the genome using a transposon-based strategy (Frokjaer-Jensen et al., 2008). Briefly, engineered transgenes were cloned into either pCFJ151 or pCF352 vectors and injected into strains EG6429 or EG6701 in order to generate single-copy insertions in chromosome II or I, respectively (Frokjaer-Jensen et al., 2008). Alternatively, transgenes cloned into pCFJ151 were injected onto strain EG8078 to obtain insertions in chromosome I (Frokjaer-Jensen et al., 2014). Transformants were selected on the basis of their ability to rescue the mobility defect of the parental strains and successful integrants were identified by PCR genotyping.

For the generation of *mad-2*, *cyb-1* and *cyb-3* transgene-based replacement systems, we engineered constructs containing the genomic locus for each gene, which included their promoter and 3'UTR (Fig. S4F; S5C). In the case of *mad-2*, intron 4 was removed because it contains repetitive sequences that made cloning and amplification difficult. All transgenes rescued the lethality of the respective null mutants (Fig. S4H; S5E). Replacement systems for MAD-1 and CDC-20 were described previously (Moyle et al., 2014; Kim et al., 2017).

CRISPR/Cas9-mediated genome editing—For the generation of *mad-2* and *mad-3* null alleles, we used a CRISPR/Cas9 strategy in which the coding sequence of each gene was replaced with the *Caenorhabditis briggsae unc-119* sequence (Fig. S1A). We engineered plasmids encoding for single-guide RNAs (sgRNA) (Table S1) along with Cas9 (pDD162; Dickinson et al., 2013), as well as donor repair constructs containing *C.b. unc-119* flanked by 2–3 kb homology arms flanking the sequence to be replaced. A mixture of these plasmids was microinjected into strain HT1593 [*unc-119(ed3)III*] and transformants selected 10 days later based on rescue of the *unc-119(ed3)* mobility defect. Genome editing was assessed by PCR, and successfully edited animals were backcrossed to N2 wild-type to remove any potential off-target mutations and balanced using either *nT1[qIs51]* for *mad-2Δ* (*mdf-2(lt4)*) or *hT2[bli-4(e937) let-?(q782) qIs48]* for *mad-3Δ* (*san-1(lt6)*). Both balancers express GFP in the pharynx in order to distinguish between homozygous mutant and heterozygous animals under a fluorescence stereomicroscope.

For the generation of a *cyb-3* null allele, we used a co-CRISPR strategy in which *dpy-10* was co-edited together with the *cyb-3* locus (Arribere et al., 2014; Kim et al., 2014; Hattersley et al., 2018). N2 wild-type worms were injected with a mixture containing purified Cas9, tracrRNA, two crRNAs flanking the *cyb-3* coding sequence and a crRNA targeting *dpy-10*. Four days later, *dpy-10* mutants (which can be distinguished by their *dumpy* or *roller* phenotypes) were selected and screened by PCR to detect edits that removed the entire *cyb-3* coding sequence, which were further confirmed by sequencing. The *cyb-3* deletion (*cyb-3(lt110)*) was then backcrossed to N2 wild-type to remove the *dpy-10* mutation and balanced using *nT1[qIs51]*.

The null allele for *cdc-20* (*fzy-1(lt20)*) was previously described (Kim et al., 2017). Null mutants for *mad-1* (*mdf-1(gk2)*) and *cyb-1* (*cyb-1(gk35)*), as well as temperature-sensitive mutants for *Apc8* (*Apc8*^{ts}; *mat-3(or334)*), *Apc6* (*Apc6*^{ts}; *emb-27(g48)*) and *cdk-1* (*cdk-1*^{ts}; *cdk-1(ne2257)*) were obtained from the Caenorhabditis Genetics Center (CGC). For the generation of *in situ* fluorescent tags for MAD-2, CYB-1 and CYB-3, we used the self-excising cassette method (SEC) (Dickinson et al., 2015). Generation of *in situ* fluorescently tagged MAD-1 was described previously (Kim et al., 2017; Wang et al., 2017).

RNA-mediated interference (RNAi)—Double-stranded RNAs (dsRNAs) used in this study are listed in Table S2. For embryo assays, dsRNAs were injected into L4 stage worms at a final concentration of 1 mg/ml. Worms were recovered at 20°C and embryos were analy zed 36–48h later. For embryonic lethality assays, L4s injected with dsRNAs were grown at 20°C for 24h, singled onto 35 mm plates and allowed to lay progeny for an additional 24h before the mothers were removed. The next day, after embryos had hatched in controls, embryonic lethality was scored.

For RNAi soaking (Tabara et al., 1998; Timmons et al., 2001), starved L1 larvae generated as described below, were transferred to a 5 μl drop of a mix containing 3.15 mM Spermidine, 0.055% gelatin and dsRNAs at a final concentration of 0.5 – 1.0 mg/ml in 1X soaking buffer (10.9 mM Na_2HPO_4, 5.5 mM KH_2PO_4, 1.26 mM NaCl and 4.7 mM NH_4Cl), under RNAse-free conditions. Between 20–50 L1s were transferred to each drop. Soaked

worms were incubated for 24h at 20°C in a humidifie d chamber, then recovered onto NGM plates with OP50 food at 20°C and imaged 7–72h late r.

Germ cell proliferation assays—For germ cell proliferation assays, L4 stage worms were injected with dsRNAs, recovered at 20°C and 24h later, adults were dissolved on NGM pl ates with no bacteria using a 50:50 mixture of 2N NaOH and concentrated household bleach. This treatment dissolves the worm bodies while leaving the embryos intact (Fig. S2A). The following day or two days later, after starved L1 larvae had hatched, worms were transferred onto NGM plates seeded with OP50 food and samples were taken every 4 or 7 hours in order to image germ cell proliferation. For experiments with the CDC-20 3A mutant, starved L1s were soaked in the indicated dsRNAs for 24h, recovered at 20°C and ima ged every 7 hours. For experiments with null mutants, balanced strains were maintained at 22°C and first homozygous generation worms were analyzed as described above.

Fertility/viability analysis—For scoring of progeny number over successive generations, mutants and, when applicable, their rescuing transgenes were maintained with balancer chromosomes (*nT1[qIs51] (IV/V)* for *mad-1Δ* and *mad-2Δ, hT2[bli-4(e937) let-?(q782) qIs48] (I,III)* for *mad-3Δ* and *mIn1[mIs14 dpy-10(e128)]II* for *cdc-20Δ*). All balancers used express GFP in the pharynx, which helps distinguish heterozygous balanced worms (GFP positive) from homozygous mutant worms (GFP negative; homozygotes for the balancer chromosome were either embryonic lethal or *dumpy*).

Balanced strains were propagated at 20°C. Homozygou s mutant L4s originating from balanced mothers (first homozygous generation, *g1*, Fig. 1D) were singled and scored for total number of progeny laid, which were phenotypically grouped into living larvae and dead embryos. Viable progeny (second homozygous generation, *g2*) were singled and scored similarly and the whole process was repeated once more (third homozygous generation, *g3*). When generation number is not indicated, the analysis was done on strains of the indicated genotype that were propagated for multiple generations.

Antibody generation—For MAD-3 antibody production, rabbits were immunized with Maltose-binding protein (MBP) fused to full-length MAD-3. Specific antibodies were affinity-purified from the sera, using MAD-3::His, in order to prevent the purification of antibodies against MBP (Desai et al., 2003). Antibody specificity was validated by western blot, against a lysate from *mad-3Δ* worms (Fig. S1B).

Immunoblotting—Gravid adult worms were transferred to tubes containing M9 buffer (22 mM KH_2PO_4, 42 mM Na_2HPO_4, 86 mM NaCl, and 1 mM $MgSO_4$•$7H_2O$), washed 4 times with M9 containing 0.1% Tween-20 and then resuspended on 1.5X sample buffer (87.5 mM Tris-HCl pH 6.8, 2.5% SDS, 150 mM DTT, 7.5% glycerol, bromophenol blue). After lysing by sonication and boiling, the equivalent of 8–12 worms was loaded onto 4–12% NuPAGE Bis-Tris Gels (Invitrogen). Proteins were then transferred to nitrocellulose membranes, probed with primary antibodies (see Key Resources Table) and detected using either horseradish (HRP)- conjugated secondary antibodies and WesternBright Sirius (Advansta) chemiluminescent substrate or, for the α-loading control, using alkaline phosphatase (AP)-conjugated secondary antibody and Western Blue® Stabilized Substrate for Alkaline

Phosphatase (Promega). Membranes were imaged using a ChemiDoc MP imaging system (BioRad). For immunoblotting of U2OS samples, cells were collected by trypsinization, washed once with 1X PBS, resuspended on 1.5X sample buffer and boiled for 5 minutes before loading onto gels.

Immunoprecipitation—*C. elegans* strains expressing either GFP::MAD-1 or MAD-2::GFP in the background of their respective null alleles were grown in liquid culture as described (Zanin et al., 2011). Worms were harvested from cultures synchronized at the gravid adult stage, flash-frozen and stored at −80°C. For each immunoprecipitation exper iment, 1g of worm pellet was used. Worms were thawed in 1 mL of lysis buffer (75 mM HEPES pH 7.4, 1.5 mM EGTA, 1.5 mM $MgCl_2$, 150 mM KCl, 15% glycerol, 0.07% NP-40, cOmplete protease inhibitor cocktail (Roche)) and lysed by sonication. Extracts were cleared by centrifugation at 20.000 g for 20 min at 4°C and the supernatants were incubated with 40 µL of pre-equilibrated GFP-Trap beads (Chromotek) for 2 hr. at 4°C. Beads were then washed 6 times with wash buffer (50 mM HEPES pH 7.4, 1.0 mM EGTA, 1.0 mM $MgCl_2$, 100 mM KCl, 10% glycerol, 0.05% NP-40, cOmplete protease inhibitor cocktail (Roche)) and eluted with 40 µL of 1.5X sample buffer (87.5 mM Tris-HCl pH 6.8, 2.5% SDS, 150 mM DTT, 7.5% glycerol, bromophenol blue). Samples were analyzed by immunoblotting, as described above.

Yeast two-hybrid analysis—Yeast-two hybrid assays were performed using the Matchmaker GAL4 Two-Hybrid System 3 (Clonetech). cDNAs encoding MAD-2, Tpr (NPP-21 in worms), CDC-20 or the various MAD-1 fragments were cloned into either pGBKT7 or pGADT7 vectors, transformed onto *Saccharomyces cerevisiae* AH109 or Y187 strains and selected on –Trp or –Leu dropout plates respectively. Transformed strains were mated, selected onto –Trp –Leu double dropout plates and interactions were tested on either –Trp –Leu –His (low stringency) or –Trp –Leu –His –Ade dropout plates (high stringency).

Brightfield imaging of larvae and adults—Strains growing on NGM plates with food were imaged using a stereo microscope (Nikon) coupled to a Dino-Eye Digital Eyepiece Camera (Dino-lite). Images were processed using a sharpening filter in Adobe Photoshop.

Fluorescence imaging of *C. elegans* embryos and germ cells—For time-lapse imaging, *C. elegans* embryos were dissected from adults in M9 media and mounted onto 2% agarose pads, covered with a coverslip and imaged at 20°C. Time-lapse imaging of one-cell embryos expressing GFP::H2b was performed on a deconvolution microscope (DeltaVision Elite; Applied Precision) equipped with a charge-coupled device camera (pco.edge 5.5 sCMOS; PCO) and a 60× 1.42NA PlanApo N objective (Olympus). 5×2µm z-stacks without binning were acquired at 10sec intervals with 2% illumination intensity (on an InsightSSI illuminator) and 100 ms exposure. Similar settings were used for imaging of monopolar mitoses in the two-cell embryo, except that a 20 sec interval imaging protocol was used.

Imaging of GFP::MAD-1 or MAD-2::GFP unattached kinetochore localization was performed on an Andor Revolution XD Confocal System (Andor Technology) with a spinning disk confocal scanner unit (CSU-10; Yokogawa) mounted on an inverted microscope (TE2000-E; Nikon), 100x or 60× 1.4 NA Plan Apochromat lenses, and outfitted

with an electron multiplication back-thinned charged-coupled device camera (iXon, Andor Technology).

For imaging of germ cells, larvae were anesthetized with a mixture containing 0.2 mg/ml Tetramisole hydrochloride; 2 mg/ml Tricane (Sigma). 15 min later, larvae were transferred to 2% agarose pads using a mouth pipette, covered with a coverslip and imaged using an Andor microscope system (see above). For L1-L2 larvae, 26 × 1 μm series were taken, whereas for L4 germlines we used 40 × 1 μm series. Images were then processed using Fiji (Schindelin et al., 2012), and cells were counted through all z-planes.

Imaging analysis—For time-lapse experiments, NEBD was scored as the frame where free histone signal in the nucleus equilibrated with the cytoplasm, which was just before abrupt chromosome movements were evident. Anaphase onset was scored as the first frame with visible separation of sister chromatids. DNA decondensation was scored as the first frame where the histone intensity diminished and its area expanded. For cell cycle staging in germ cells, nuclei were scored as being in S-phase when the GFP::PCNA^{PCN-1} fluorescence was bright and punctate, or being in G2 when GFP::PCNA^{PCN-1} was dim and diffused. For quantification of GFP::MAD-1 and MAD-2::GFP nuclear periphery signals, images were imported to Fiji and a line-scan method was used (see Fig. S3G for details).

Cell cycle analysis of human U2OS cells—U2OS cells expressing GFP-PCNA and H2B-mRFP were previously described (de Groot et al., 2015). Cells growing at a 40–60% confluency were transfected with a mixture of siRNA oligos targeting the Mad2 3'-UTR (Ye et al., 2017), an ON-TARGET*plus* siRNA mix for BubR1 or a non-targeting siRNA mixture as a control (Dharmacon) at a final concentration of 100 nM using Lipofectamine RNAiMAX (Thermo Fisher). 24h after transfection, cells were seeded onto a 96-well microplate (Greiner, Cat. #655866); if used, RO-3306 (Vassilev et al., 2006) was added to a final concentration of 5 μM at this time. Movies were acquired on a CV1000 spinning disk confocal system (Yokogawa) with a 20x U-PlanApo 0.75 NA objective and 512×512 EM-CCD camera (Hamamatsu). Image acquisition and data analysis were performed using CellVoyager software. The humidity-controlled imaging chamber was maintained at 37°C and 5% CO_2. 4 fields per well were imaged and a 2×2 binning protocol was used. 4 × 3 μm z-sections in the GFP (20% power, 250 ms, 25% gain) and RFP (20% power, 150 ms, 25% gain) channels were captured in each field at 10-minute intervals for 60 hours. Cells were manually tracked from the disappearance of GFP-PCNA foci to the beginning of the next mitosis (nuclear envelope breakdown). GFP-PCNA foci appear in the nucleus during mid to late S-phase, and the first frame in which these foci are no longer visible was defined as the beginning of G2 phase. Results represent combined measurements of a minimum of 100 cells per condition from two independent experiments.

For spindle checkpoint assays, cells were treated with nocodazole (Sigma) at a final concentration of 0.2 μg/ml and imaged under similar conditions as described above, except that 5 minute intervals were used. Mitotic duration was determined as the interval between nuclear envelope breakdown and DNA decondensation.

Generation of lentivirus-expressed Myc-Mad2 cell line—For Mad2 siRNA rescue experiments, a Myc-Mad2 cDNA was cloned into a lentiviral vector, under the PGK promoter. The vector also contains a P2A sequence followed by a Blasticidin S deaminase gene for the selection of positive integrants using Blasticidin. Lentiviruses were generated using the Lenti-X Packaging Single Shots (VSV-G; Takara), following the manufacturer's instructions. Viruses were used to infect U2OS cells expressing GFP-PCNA and H2b-mRFP and 48 h later, cells were treated with 10 μg/mL Blasticidin-S HCl (Gibco) until the appearance of resistant colonies. The polyclonal population was tested for expression of Myc-Mad2 and used for analysis.

Generation of *in situ* mNeongreen-tagged cyclin B1 cell line—For the generation of cyclin B1-mNeonGreen, a CRISPR-Cas9 strategy was used. Briefly, we engineered a construct encoding ~1000 bp of left homology arm corresponding to the cyclin B1 C-terminus, fused to the linker ASKLGAGAGAGAGAGAG and followed by the coding sequence for mNeonGreen. The construct also contained a P2A ribosome skipping peptide, a Neomycin resistance cassette downstream of the mNeonGreen sequence and 600 bp of right homology arm corresponding to the cyclin B1 3'-UTR (Fig. S5G).

U2OS cells were nucleofected with a mixture containing this construct and a plasmid encoding Cas9 and the gRNA targeting sequence ((pX459; Ran et al., 2013); Table S1) using Cell Line Nucleofector Solution V (Lonza). Two days after nucleofection, cells were seeded onto 96-well plates and selected using 400 μg/mL of G418 (Gibco). After two weeks, when colonies became visible, clones were transferred to 24-well plates, screened by immunoblotting with an anti-Cyclin B1 antibody (see Key Resources Table) to identify clones where endogenous cyclin B1 was replaced by cyclin B1-mNeonGreen. Selected clones were further subjected to sequencing and PCR genotyping (see Fig. S5H).

Cyclin B1 accumulation assays—U2OS cells expressing *in situ* mNeongreen-tagged cyclin B1 were transfected with siRNAs as described above and transferred to 96-well plates (Greiner, Cat. #655866). Two hours before imaging, SiR-DNA (Cytoskeleton, Inc) was added to a final concentration of 0.5 μM. Imaging was performed on a CQ-1 spinning disk confocal system (Yokogawa) with a 40x UPLSAPO 40×2 0.95 NA objective and a 2560 × 2160 pixel sCMOS camera. Image acquisition and data analysis were performed using CellVoyager software. The humidity-controlled imaging chamber was maintained at 37°C a nd 5% CO_2. 6 fields per well were imaged and a 2×2 binning protocol was used. 6 × 3 μm z-sections in the 488 nm (25% power, 300 ms) and 640 nm (25% power, 100 ms) channels were captured in each field at 10-minute intervals for 48 hours.

For quantification of cyclin B1 accumulation, maximum intensity projections were generated using Fiji (Schindelin et al., 2012). An area was manually drawn around the entire cell and measured over time. The same area was copied to a region of the field with no cells in order to measure background. Background-corrected intensities were plotted relative to nuclear envelope breakdown using Prism (Graphpad).

Quantification And Statistical Analysis

Statistical parameters are reported in the Figures and Figure Legends. In figures, asterisks denote statistical significance as calculated by Mann-Whitney or Kolmogorov-Smirnov tests (•, $p < 0.05$; ••, $p < 0.01$; •••, $p < 0.001$; ••••, $p < 0.0001$). Statistical analysis was performed using Prism (Graphpad).

Data Code And Availability

This study did not generate datasets or code.

Supplementary Material

Refer to Web version on PubMed Central for supplementary material.

ACKNOWLEDGEMENTS:

We thank the Caenorhabditis Genetics Center for providing mutant strains; Rebecca Green for help with germline analyses; Dong Hyun Kim, Ruth Kabeche, Franz Meitinger and David Jenkins for advice on human cell experiments; Stephen Taylor and Don Cleveland for antibodies, Kevin Corbett for APC/C schematics and comments on the manuscript and Jonathon Pines for helpful discussions. This work was supported by an NIH grant (GM074215) to A.D. P.L-G. was supported by a Pew Latin American fellowship. A.D. and K.O. receive salary and other support from the Ludwig Institute for Cancer Research.

REFERENCES

Alfieri C, Chang L, Zhang Z, Yang J, Maslen S, Skehel M, and Barford D (2016). Molecular basis of APC/C regulation by the spindle assembly checkpoint. Nature 536, 431–436. [PubMed: 27509861]

Alfieri C, Zhang S, and Barford D (2017). Visualizing the complex functions and mechanisms of the anaphase promoting complex/cyclosome (APC/C). Open Biol 7.

Arribere JA, Bell RT, Fu BX, Artiles KL, Hartman PS, and Fire AZ (2014). Efficient marker-free recovery of custom genetic modifications with CRISPR/Cas9 in Caenorhabditis elegans. Genetics 198, 837–846. [PubMed: 25161212]

Campbell MS, Chan GK, and Yen TJ (2001). Mitotic checkpoint proteins HsMAD1 and HsMAD2 are associated with nuclear pore complexes in interphase. J Cell Sci 114, 953–963. [PubMed: 11181178]

Chen RH, Shevchenko A, Mann M, and Murray AW (1998). Spindle checkpoint protein Xmad1 recruits Xmad2 to unattached kinetochores. J Cell Biol 143, 283–295. [PubMed: 9786942]

Chung E, and Chen RH (2002). Spindle checkpoint requires Mad1-bound and Mad1-free Mad2. Mol Biol Cell 13, 1501–1511. [PubMed: 12006648]

Clute P, and Pines J (1999). Temporal and spatial control of cyclin B1 destruction in metaphase. Nat Cell Biol 1, 82–87. [PubMed: 10559878]

Corbett KD (2017). Molecular Mechanisms of Spindle Assembly Checkpoint Activation and Silencing. Prog Mol Subcell Biol 56, 429–455. [PubMed: 28840248]

De Antoni A, Pearson CG, Cimini D, Canman JC, Sala V, Nezi L, Mapelli M, Sironi L, Faretta M, Salmon ED, et al. (2005). The Mad1/Mad2 complex as a template for Mad2 activation in the spindle assembly checkpoint. Curr Biol 15, 214–225. [PubMed: 15694304]

de Groot CO, Hsia JE, Anzola JV, Motamedi A, Yoon M, Wong YL, Jenkins D, Lee HJ, Martinez MB, Davis RL, et al. (2015). A Cell Biologist's Field Guide to Aurora Kinase Inhibitors. Front Oncol 5, 285. [PubMed: 26732741]

Desai A, Rybina S, Muller-Reichert T, Shevchenko A, Shevchenko A, Hyman A, and Oegema K (2003). KNL-1 directs assembly of the microtubule-binding interface of the kinetochore in C. elegans. Genes Dev 17, 2421–2435. [PubMed: 14522947]

Di Fiore B, and Pines J (2007). Emi1 is needed to couple DNA replication with mitosis but does not regulate activation of the mitotic APC/C. J Cell Biol 177, 425–437. [PubMed: 17485488]

Dickinson DJ, Pani AM, Heppert JK, Higgins CD, and Goldstein B (2015). Streamlined Genome Engineering with a Self-Excising Drug Selection Cassette. Genetics 200, 1035–1049. [PubMed: 26044593]

Dickinson DJ, Ward JD, Reiner DJ, and Goldstein B (2013). Engineering the Caenorhabditis elegans genome using Cas9-triggered homologous recombination. Nat Methods 10, 1028–1034. [PubMed: 23995389]

Edgar BA, and Orr-Weaver TL (2001). Endoreplication cell cycles: more for less. Cell 105, 297–306. [PubMed: 11348589]

Essex A, Dammermann A, Lewellyn L, Oegema K, and Desai A (2009). Systematic analysis in Caenorhabditis elegans reveals that the spindle checkpoint is composed of two largely independent branches. Mol Biol Cell 20, 1252–1267. [PubMed: 19109417]

Faesen AC, Thanasoula M, Maffini S, Breit C, Muller F, van Gerwen S, Bange T, and Musacchio A (2017). Basis of catalytic assembly of the mitotic checkpoint complex. Nature 542, 498–502. [PubMed: 28102834]

Fang G (2002). Checkpoint protein BubR1 acts synergistically with Mad2 to inhibit anaphase-promoting complex. Mol Biol Cell 13, 755–766. [PubMed: 11907259]

Ferrell JE Jr. (2013). Feedback loops and reciprocal regulation: recurring motifs in the systems biology of the cell cycle. Curr Opin Cell Biol 25, 676–686. [PubMed: 23927869]

Fox PM, Vought VE, Hanazawa M, Lee MH, Maine EM, and Schedl T (2011). Cyclin E and CDK-2 regulate proliferative cell fate and cell cycle progression in the C. elegans germline. Development 138, 2223–2234. [PubMed: 21558371]

Frokjaer-Jensen C, Davis MW, Hopkins CE, Newman BJ, Thummel JM, Olesen SP, Grunnet M, and Jorgensen EM (2008). Single-copy insertion of transgenes in Caenorhabditis elegans. Nature genetics 40, 1375–1383. [PubMed: 18953339]

Frokjaer-Jensen C, Davis MW, Sarov M, Taylor J, Flibotte S, LaBella M, Pozniakovsky A, Moerman DG, and Jorgensen EM (2014). Random and targeted transgene insertion in Caenorhabditis elegans using a modified Mos1 transposon. Nat Methods 11, 529–534. [PubMed: 24820376]

Fujimitsu K, Grimaldi M, and Yamano H (2016). Cyclin-dependent kinase 1-dependent activation of APC/C ubiquitin ligase. Science 352, 1121–1124. [PubMed: 27103671]

Fukuyama M, Rougvie AE, and Rothman JH (2006). C. elegans DAF-18/PTEN mediates nutrient-dependent arrest of cell cycle and growth in the germline. Curr Biol 16, 773–779. [PubMed: 16631584]

Golden A, Sadler PL, Wallenfang MR, Schumacher JM, Hamill DR, Bates G, Bowerman B, Seydoux G, and Shakes DC (2000). Metaphase to anaphase (mat) transition-defective mutants in Caenorhabditis elegans. J Cell Biol 151, 1469–1482. [PubMed: 11134076]

Gopinathan L, Szmyd R, Low D, Diril MK, Chang HY, Coppola V, Liu K, Tessarollo L, Guccione E, van Pelt AMM, et al. (2017). Emi2 Is Essential for Mouse Spermatogenesis. Cell Rep 20, 697–708. [PubMed: 28723571]

Green RA, Kao HL, Audhya A, Arur S, Mayers JR, Fridolfsson HN, Schulman M, Schloissnig S, Niessen S, Laband K, et al. (2011). A high-resolution C. elegans essential gene network based on phenotypic profiling of a complex tissue. Cell 145, 470–482. [PubMed: 21529718]

Grosskortenhaus R, and Sprenger F (2002). Rca1 inhibits APC-Cdh1(Fzr) and is required to prevent cyclin degradation in G2. Dev Cell 2, 29–40. [PubMed: 11782312]

Hattersley N, Lara-Gonzalez P, Cheerambathur D, Gomez-Cavazos JS, Kim T, Prevo B, Khaliullin R, Lee KY, Ohta M, Green R, et al. (2018). Employing the one-cell C. elegans embryo to study cell division processes. Methods Cell Biol 144, 185–231. [PubMed: 29804670]

Hein JB, and Nilsson J (2016). Interphase APC/C-Cdc20 inhibition by cyclin A2-Cdk2 ensures efficient mitotic entry. Nat Commun 7, 10975. [PubMed: 26960431]

Hwang LH, Lau LF, Smith DL, Mistrot CA, Hardwick KG, Hwang ES, Amon A, and Murray AW (1998). Budding yeast Cdc20: a target of the spindle checkpoint. Science 279, 1041–1044. [PubMed: 9461437]

Izawa D, and Pines J (2012). Mad2 and the APC/C compete for the same site on Cdc20 to ensure proper chromosome segregation. J Cell Biol 199, 27–37. [PubMed: 23007648]

Izawa D, and Pines J (2015). The mitotic checkpoint complex binds a second CDC20 to inhibit active APC/C. Nature 517, 631–634. [PubMed: 25383541]

Janssen A, and Medema RH (2013). Genetic instability: tipping the balance. Oncogene 32, 4459–4470. [PubMed: 23246960]

Jaspersen SL, Charles JF, and Morgan DO (1999). Inhibitory phosphorylation of the APC regulator Hct1 is controlled by the kinase Cdc28 and the phosphatase Cdc14. Curr Biol 9, 227–236. [PubMed: 10074450]

Kim DH, Han JS, Ly P, Ye Q, McMahon MA, Myung K, Corbett KD, and Cleveland DW (2018). TRIP13 and APC15 drive mitotic exit by turnover of interphase- and unattached kinetochore-produced MCC. Nat Commun 9, 4354. [PubMed: 30341343]

Kim H, Ishidate T, Ghanta KS, Seth M, Conte D Jr., Shirayama M, and Mello CC (2014). A co-CRISPR strategy for efficient genome editing in Caenorhabditis elegans. Genetics 197, 1069–1080. [PubMed: 24879462]

Kim T, Lara-Gonzalez P, Prevo B, Meitinger F, Cheerambathur DK, Oegema K, and Desai A (2017). Kinetochores accelerate or delay APC/C activation by directing Cdc20 to opposing fates. Genes Dev 31, 1089–1094. [PubMed: 28698300]

Kim T, Moyle MW, Lara-Gonzalez P, De Groot C, Oegema K, and Desai A (2015). Kinetochore-localized BUB-1/BUB-3 complex promotes anaphase onset in C. elegans. J Cell Biol 209, 507–517. [PubMed: 25987605]

Kitagawa R, Law E, Tang L, and Rose AM (2002). The Cdc20 homolog, FZY-1, and its interacting protein, IFY-1, are required for proper chromosome segregation in Caenorhabditis elegans. Curr Biol 12, 2118–2123. [PubMed: 12498686]

Kitagawa R, and Rose AM (1999). Components of the spindle-assembly checkpoint are essential in Caenorhabditis elegans. Nat Cell Biol 1, 514–521. [PubMed: 10587648]

Kreutzer MA, Richards JP, De Silva-Udawatta MN, Temenak JJ, Knoblich JA, Lehner CF, and Bennett KL (1995). Caenorhabditis elegans cyclin A- and B-type genes: a cyclin A multigene family, an ancestral cyclin B3 and differential germline expression. J Cell Sci 108 (Pt 6), 2415–2424. [PubMed: 7545687]

Kulukian A, Han JS, and Cleveland DW (2009). Unattached kinetochores catalyze production of an anaphase inhibitor that requires a Mad2 template to prime Cdc20 for BubR1 binding. Dev Cell 16, 105–117. [PubMed: 19154722]

Labit H, Fujimitsu K, Bayin NS, Takaki T, Gannon J, and Yamano H (2012). Dephosphorylation of Cdc20 is required for its C-box-dependent activation of the APC/C. EMBO J 31, 3351–3362. [PubMed: 22713866]

Lara-Gonzalez P, Kim T, and Desai A (2017). Taming the Beast: Control of APC/C(Cdc20)-Dependent Destruction. Cold Spring Harb Symp Quant Biol 82, 111–121. [PubMed: 29133301]

Lee SH, Sterling H, Burlingame A, and McCormick F (2008). Tpr directly binds to Mad1 and Mad2 and is important for the Mad1-Mad2-mediated mitotic spindle checkpoint. Genes Dev 22, 2926–2931. [PubMed: 18981471]

Leonhardt H, Rahn HP, Weinzierl P, Sporbert A, Cremer T, Zink D, and Cardoso MC (2000). Dynamics of DNA replication factories in living cells. J Cell Biol 149, 271–280. [PubMed: 10769021]

Luo X, Tang Z, Rizo J, and Yu H (2002). The Mad2 spindle checkpoint protein undergoes similar major conformational changes upon binding to either Mad1 or Cdc20. Mol Cell 9, 59–71. [PubMed: 11804586]

Machida YJ, and Dutta A (2007). The APC/C inhibitor, Emi1, is essential for prevention of rereplication. Genes Dev 21, 184–194. [PubMed: 17234884]

Malureanu LA, Jeganathan KB, Hamada M, Wasilewski L, Davenport J, and van Deursen JM (2009). BubR1 N terminus acts as a soluble inhibitor of cyclin B degradation by APC/C(Cdc20) in interphase. Dev Cell 16, 118–131. [PubMed: 19154723]

Morgan DO (2007). The cell cycle : principles of control (Sunderland, MA: Oxford University Press).

Morgan DO (2016). Cell division: Mitotic regulation comes into focus. Nature 536, 407–408. [PubMed: 27509855]

Moyle MW, Kim T, Hattersley N, Espeut J, Cheerambathur DK, Oegema K, and Desai A (2014). A Bub1-Mad1 interaction targets the Mad1-Mad2 complex to unattached kinetochores to initiate the spindle checkpoint. J Cell Biol 204, 647–657. [PubMed: 24567362]

Musacchio A (2015). The Molecular Biology of Spindle Assembly Checkpoint Signaling Dynamics. Curr Biol 25, R1002–1018. [PubMed: 26485365]

Peters JM (2006). The anaphase promoting complex/cyclosome: a machine designed to destroy. Nat Rev Mol Cell Biol 7, 644–656. [PubMed: 16896351]

Pines J (2011). Cubism and the cell cycle: the many faces of the APC/C. Nat Rev Mol Cell Biol 12, 427–438. [PubMed: 21633387]

Qiao R, Weissmann F, Yamaguchi M, Brown NG, VanderLinden R, Imre R, Jarvis MA, Brunner MR, Davidson IF, Litos G, et al. (2016). Mechanism of APC/CCDC20 activation by mitotic phosphorylation. Proc Natl Acad Sci U S A 113, E2570–2578. [PubMed: 27114510]

Ran FA, Hsu PD, Wright J, Agarwala V, Scott DA, and Zhang F (2013). Genome engineering using the CRISPR-Cas9 system. Nat Protoc 8, 2281–2308. [PubMed: 24157548]

Rappleye CA, Tagawa A, Lyczak R, Bowerman B, and Aroian RV (2002). The anaphase-promoting complex and separin are required for embryonic anterior-posterior axis formation. Dev Cell 2, 195–206. [PubMed: 11832245]

Reimann JD, Freed E, Hsu JY, Kramer ER, Peters JM, and Jackson PK (2001). Emi1 is a mitotic regulator that interacts with Cdc20 and inhibits the anaphase promoting complex. Cell 105, 645–655. [PubMed: 11389834]

Rodriguez-Bravo V, Maciejowski J, Corona J, Buch HK, Collin P, Kanemaki MT, Shah JV, and Jallepalli PV (2014). Nuclear pores protect genome integrity by assembling a premitotic and Mad1-dependent anaphase inhibitor. Cell 156, 1017–1031. [PubMed: 24581499]

Schindelin J, Arganda-Carreras I, Frise E, Kaynig V, Longair M, Pietzsch T, Preibisch S, Rueden C, Saalfeld S, Schmid B, et al. (2012). Fiji: an open-source platform for biological-image analysis. Nat Methods 9, 676–682. [PubMed: 22743772]

Schmidt A, Duncan PI, Rauh NR, Sauer G, Fry AM, Nigg EA, and Mayer TU (2005). Xenopus polo-like kinase Plx1 regulates XErp1, a novel inhibitor of APC/C activity. Genes Dev 19, 502–513. [PubMed: 15713843]

Schwab M, Lutum AS, and Seufert W (1997). Yeast Hct1 is a regulator of Clb2 cyclin proteolysis. Cell 90, 683–693. [PubMed: 9288748]

Scott RJ, Lusk CP, Dilworth DJ, Aitchison JD, and Wozniak RW (2005). Interactions between Mad1p and the nuclear transport machinery in the yeast Saccharomyces cerevisiae. Mol Biol Cell 16, 4362–4374. [PubMed: 16000377]

Seidel HS, and Kimble J (2015). Cell-cycle quiescence maintains Caenorhabditis elegans germline stem cells independent of GLP-1/Notch. Elife 4.

Shah JV, Botvinick E, Bonday Z, Furnari F, Berns M, and Cleveland DW (2004). Dynamics of centromere and kinetochore proteins; implications for checkpoint signaling and silencing. Curr Biol 14, 942–952. [PubMed: 15182667]

Shirayama M, Soto MC, Ishidate T, Kim S, Nakamura K, Bei Y, van den Heuvel S, and Mello CC (2006). The Conserved Kinases CDK-1, GSK-3, KIN-19, and MBK-2 Promote OMA-1 Destruction to Regulate the Oocyte-to-Embryo Transition in C. elegans. Curr Biol 16, 47–55. [PubMed: 16343905]

Sironi L, Mapelli M, Knapp S, De Antoni A, Jeang KT, and Musacchio A (2002). Crystal structure of the tetrameric Mad1-Mad2 core complex: implications of a ‘safety belt’ binding mechanism for the spindle checkpoint. EMBO J 21, 2496–2506. [PubMed: 12006501]

Stein KK, Davis ES, Hays T, and Golden A (2007). Components of the spindle assembly checkpoint regulate the anaphase-promoting complex during meiosis in Caenorhabditis elegans. Genetics 175, 107–123. [PubMed: 17057243]

Tabara H, Grishok A, and Mello CC (1998). RNAi in C. elegans: soaking in the genome sequence. Science 282, 430–431. [PubMed: 9841401]

Tang Z, Bharadwaj R, Li B, and Yu H (2001). Mad2-Independent inhibition of APCCdc20 by the mitotic checkpoint protein BubR1. Dev Cell 1, 227–237. [PubMed: 11702782]

Tarailo-Graovac M, Wang J, Tu D, Baillie DL, Rose AM, and Chen N (2010). Duplication of cyb-3 (cyclin B3) suppresses sterility in the absence of mdf-1/MAD1 spindle assembly checkpoint component in Caenorhabditis elegans. Cell Cycle 9, 4858–4865. [PubMed: 21131781]

Tighe A, Staples O, and Taylor S (2008). Mps1 kinase activity restrains anaphase during an unperturbed mitosis and targets Mad2 to kinetochores. J Cell Biol 181, 893–901. [PubMed: 18541701]

Timmons L, Court DL, and Fire A (2001). Ingestion of bacterially expressed dsRNAs can produce specific and potent genetic interference in Caenorhabditis elegans. Gene 263, 103–112. [PubMed: 11223248]

Tung JJ, Hansen DV, Ban KH, Loktev AV, Summers MK, Adler JR 3rd, and Jackson PK (2005). A role for the anaphase-promoting complex inhibitor Emi2/XErp1, a homolog of early mitotic inhibitor 1, in cytostatic factor arrest of Xenopus eggs. Proc Natl Acad Sci U S A 102, 4318–4323. [PubMed: 15753281]

van der Voet M, Lorson MA, Srinivasan DG, Bennett KL, and van den Heuvel S (2009). C. elegans mitotic cyclins have distinct as well as overlapping functions in chromosome segregation. Cell Cycle 8, 4091–4102. [PubMed: 19829076]

Vassilev LT, Tovar C, Chen S, Knezevic D, Zhao X, Sun H, Heimbrook DC, and Chen L (2006). Selective small-molecule inhibitor reveals critical mitotic functions of human CDK1. Proc Natl Acad Sci U S A 103, 10660–10665. [PubMed: 16818887]

Visintin R, Prinz S, and Amon A (1997). CDC20 and CDH1: a family of substrate-specific activators of APC-dependent proteolysis. Science 278, 460–463. [PubMed: 9334304]

Wang S, Tang NH, Lara-Gonzalez P, Zhao Z, Cheerambathur DK, Prevo B, Chisholm AD, Desai A, and Oegema K (2017). A toolkit for GFP-mediated tissue-specific protein degradation in C. elegans. Development 144, 2694–2701. [PubMed: 28619826]

Wang S, Wu D, Quintin S, Green RA, Cheerambathur DK, Ochoa SD, Desai A, and Oegema K (2015). NOCA-1 functions with gamma-tubulin and in parallel to Patronin to assemble non-centrosomal microtubule arrays in C. elegans. Elife 4, e08649. [PubMed: 26371552]

Wolthuis R, Clay-Farrace L, van Zon W, Yekezare M, Koop L, Ogink J, Medema R, and Pines J (2008). Cdc20 and Cks direct the spindle checkpoint-independent destruction of cyclin A. Mol Cell 30, 290–302. [PubMed: 18471975]

Yam CH, Fung TK, and Poon RY (2002). Cyclin A in cell cycle control and cancer. Cell Mol Life Sci 59, 1317–1326. [PubMed: 12363035]

Yamaguchi M, VanderLinden R, Weissmann F, Qiao R, Dube P, Brown NG, Haselbach D, Zhang W, Sidhu SS, Peters JM, et al. (2016). Cryo-EM of Mitotic Checkpoint Complex-Bound APC/C Reveals Reciprocal and Conformational Regulation of Ubiquitin Ligation. Mol Cell 63, 593–607. [PubMed: 27522463]

Ye Q, Kim DH, Dereli I, Rosenberg SC, Hagemann G, Herzog F, Toth A, Cleveland DW, and Corbett KD (2017). The AAA+ ATPase TRIP13 remodels HORMA domains through N-terminal engagement and unfolding. EMBO J 36, 2419–2434. [PubMed: 28659378]

Yoon S, Kawasaki I, and Shim YH (2012). CDC-25.1 controls the rate of germline mitotic cell cycle by counteracting WEE-1.3 and by positively regulating CDK-1 in Caenorhabditis elegans. Cell Cycle 11, 1354–1363. [PubMed: 22421141]

Yudkovsky Y, Shteinberg M, Listovsky T, Brandeis M, and Hershko A (2000). Phosphorylation of Cdc20/fizzy negatively regulates the mammalian cyclosome/APC in the mitotic checkpoint. Biochem Biophys Res Commun 271, 299–304. [PubMed: 10799291]

Zachariae W, Schwab M, Nasmyth K, and Seufert W (1998). Control of cyclin ubiquitination by CDK-regulated binding of Hct1 to the anaphase promoting complex. Science 282, 1721–1724. [PubMed: 9831566]

Zanin E, Dumont J, Gassmann R, Cheeseman I, Maddox P, Bahmanyar S, Carvalho A, Niessen S, Yates JR 3rd, Oegema K, et al. (2011). Affinity purification of protein complexes in C. elegans. Methods Cell Biol 106, 289–322. [PubMed: 22118282]

Zhang S, Chang L, Alfieri C, Zhang Z, Yang J, Maslen S, Skehel M, and Barford D (2016). Molecular mechanism of APC/C activation by mitotic phosphorylation. Nature 533, 260–264. [PubMed: 27120157]

Highlights

- The spindle checkpoint protein Mad2 has a conserved role in the G2-to-M transition
- Mad2's role in G2-to-M requires Mad1 but is independent of kinetochores
- Mad2 enables cyclin B accumulation by restraining its degradation by APC/C-Cdc20
- Mad2 and Cdk phosphorylation act in parallel to inhibit APC/C-Cdc20 in G2

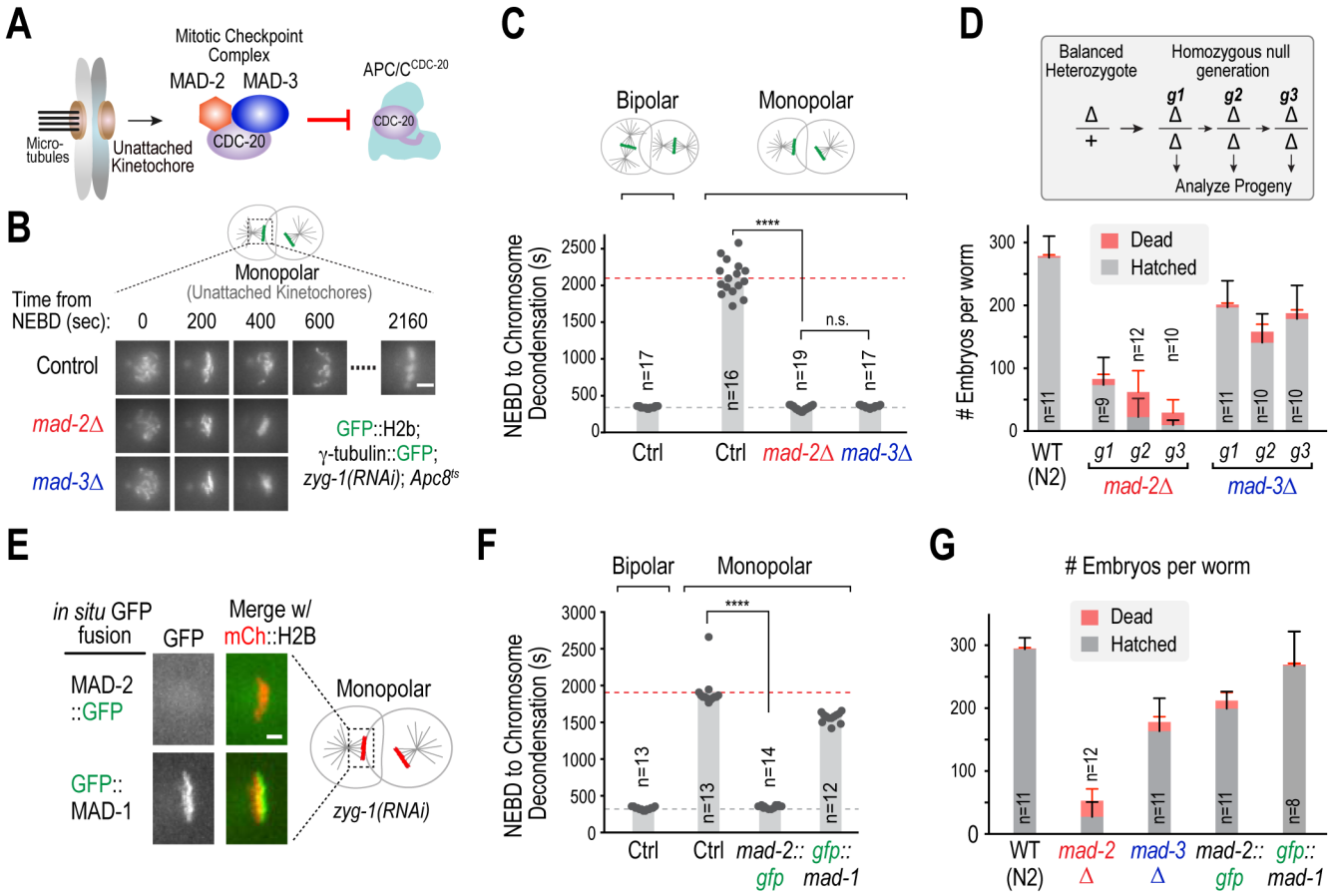

Figure 1. Mad2 contributes to viability and fertility independently of the kinetochore-activated spindle checkpoint.

(A) Schematic of spindle checkpoint signaling: unattached kinetochores generate the mitotic checkpoint complex, containing Mad2 and Mad3, that inhibits APC/C^{Cdc20}. **(B)** Spindle checkpoint assay in *C. elegans* embryos. Null embryos for *mad-2* or *mad-3* were depleted of ZYG-1, an essential centriole duplication component, in order to generate monopolar spindles in the second embryonic division. Combining this treatment with a weak APC/C mutant (*Apc8*^{ts}) results in a robust checkpoint-dependent mitotic arrest. Images show example stills of two-cell embryos undergoing mitosis under the indicated conditions. Scale bar, 5 μm. **(C)** Quantification of mitotic duration for the conditions in 1B. *n* is number of embryos scored. **(D)** Fertility and embryo viability analysis of first, second and third homozygous mutant generations (*g1*, *g2* and *g3*). *n* is number of adults whose progeny were scored. Error bars are 95% confidence intervals. **(E)** Localization of indicated in situ tagged GFP fusions to unattached kinetochores on monopolar spindles. The GFP tag interferes with the ability of MAD-2 to localize to unattached kinetochores. Scale bar, 2 μm. **(F)** & **(G)** Spindle assembly checkpoint assay *(F)* and viability and fertility analysis *(G)* for the indicated conditions. Progeny from long-term propagated strains (>3 generations) were analyzed. *n* is the number of adults scored for progeny number. Error bars are 95% confidence intervals. **** represents $p<0.0001$ from Mann-Whitney tests; non-significant (n.s.) is $p>0.05$. *See also* Figure S1.

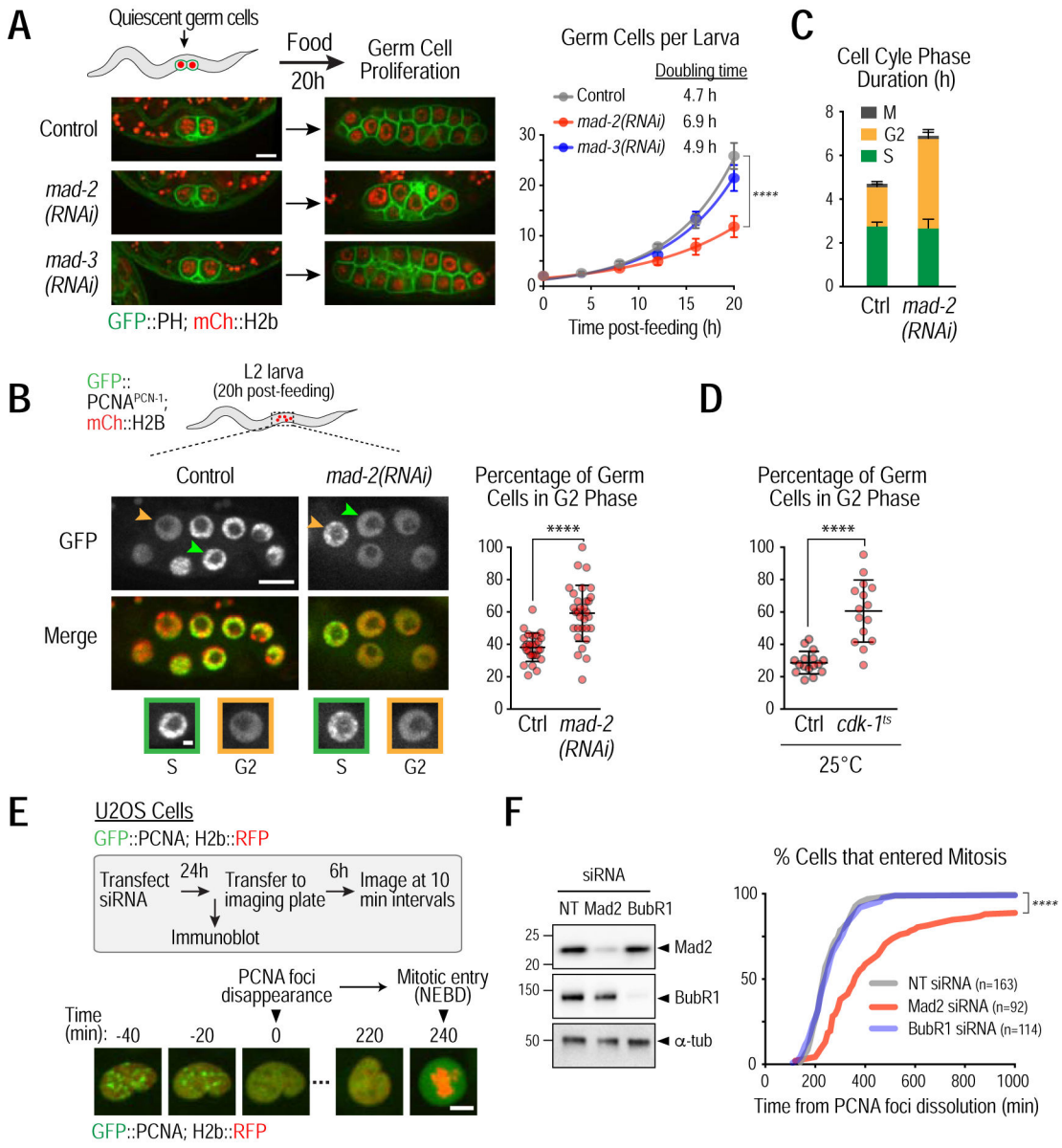

Figure 2. Mad2 promotes the G2 to M transition.

(A) Representative images *(left)* and quantification *(right)* of germ cell proliferation in the indicated conditions; germ cells are visualized using plasma membrane (GFP::PH) and chromatin (mCherry::H2b) markers expressed under a germ cell-specific promoter. >17 larvae were analyzed for each time point. Bar, 5 μm. **(B)** *(left)* Cell cycle phase analysis of germ cells, based on GFP::PCNA^{PCN-1} nuclear localization. Representative images of L2 larvae; arrowheads point to S (orange) and G2 (green) phase germ cells that are magnified in insets below. Bar, 5 μm; inset bar, 1 μm. *(right)* Quantification of proportion of G2 phase nuclei in individual larval germlines. **(C)** Duration of S and G2 phases calculated based on doubling times from Fig. 2B. **(D)** Quantification of proportion of G2 phase nuclei in individual larval germlines in the presence or absence of a weakening *cdk-1* mutation (*cdk-1^{ts}*). Experiments were done at the restrictive temperature of 25°C. **(E)** *(top)* Schematic

of G2-to-M transition analysis in human U2OS cells and *(bottom)* stills from a time-lapse movie of the nuclear region in a single cell. The time between dissolution of PCNA foci and nuclear envelope breakdown (NEBD) provides a quantitative measure for the G2-to-M transition in single cells. Bar, 10 μm. **(F)** *(left)* Immunoblot assessing protein depletion efficiency in human U2OS cells. NT is a non-targeting siRNA used as a control. BubR1 is the human orthologue of MAD-3. α-tubulin serves as a loading control. *(right)* Percent cells in mitosis as a function of time after PCNA foci dissolution for the indicated conditions. Error bars are 95% confidence intervals *(A,C)* or standard deviation *(B,D)*. **** represents $p<0.0001$ from Mann-Whitney tests *(A,B,D)* or Kolmogorov-Smirnov test *(F)*; non-significant (n.s.) is $p>0.05$. *See also* Figure S2.

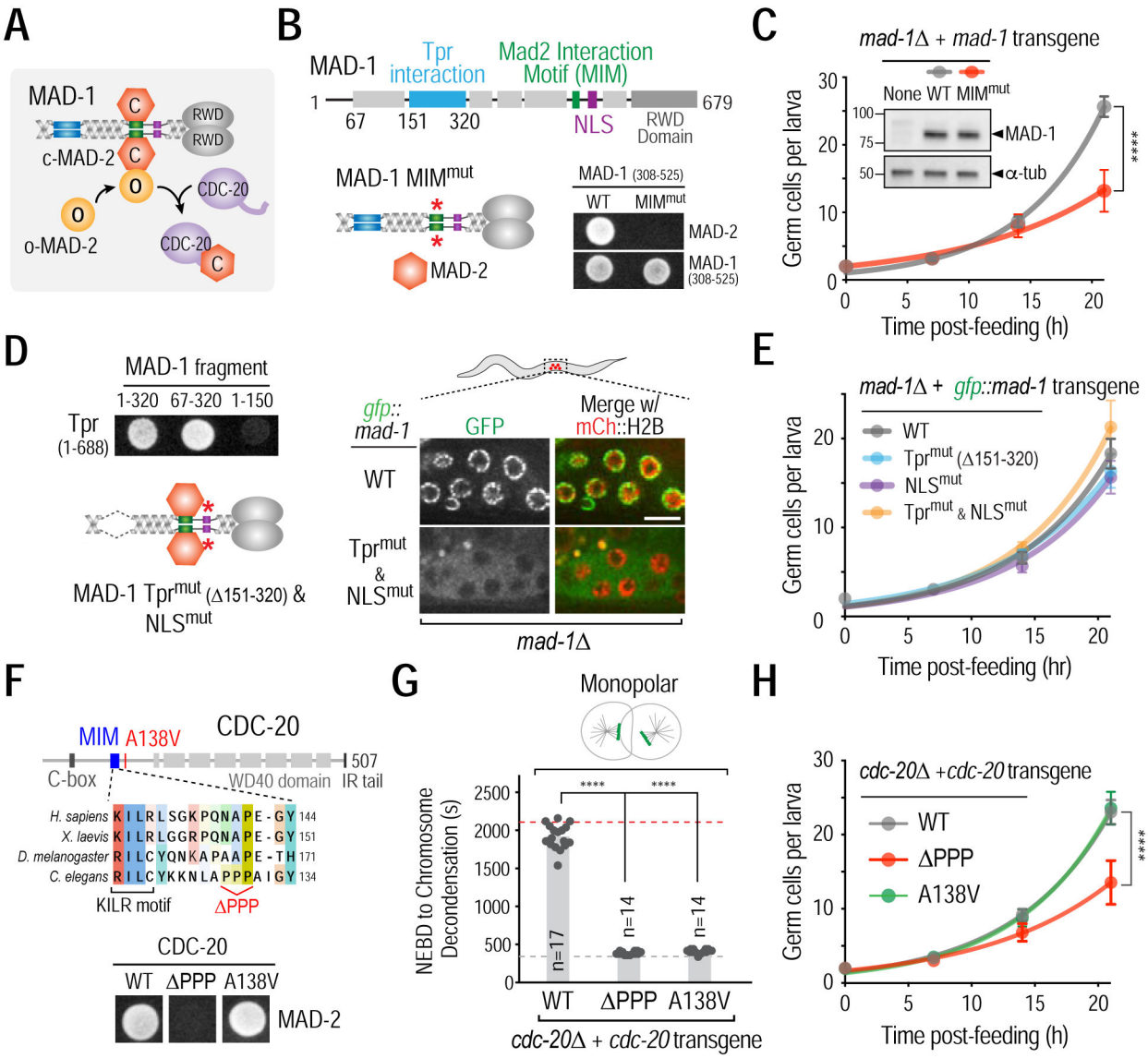

Figure 3. Mad1-Mad2 targets Cdc20 in the cytoplasm to promote the G2-to-M transition.

(A) Schematic of Mad1-Mad2-mediated catalysis of Mad2-Cdc20 complex formation. **(B)** *(top)* Schematic of MAD-1 primary structure highlighting MAD-2 interaction motif (MIM, green), Tpr interaction domain (sky blue), and nuclear localization signal (NLS, purple). *(bottom left)* Schematic of MIM^{mut} MAD-1; see Fig. S3A for details on MIM mutant generation; (*bottom right*) Yeast two-hybrid data showing the effect of mutating the MIM in MAD-1. **(C)** Effect of mutating MAD-1's MIM on germ cell proliferation. Inset shows immunoblot of *mad-1Δ* strains expressing WT or MIM^{mut} MAD-1 from single copy transgene insertions. α-tubulin serves as a loading control**. (D)** *(left top)* Yeast two hybrid data mapping the interaction of MAD-1 with Tpr (NPP-21) to residues 151–320 and *(left bottom)* schematic of MAD-1 mutant engineered to disrupt Tpr interaction and nuclear transport; see Fig. S3A for details on NLS mutant generation; *(right)* Disruption of MAD-1 nuclear periphery and nuclear interior localization in germ cells by deletion of the Tpr interaction domain and mutation of the NLS. Bar, 5 μm. **(E)** Effect of disrupting MAD-1

nuclear periphery and/or nuclear interior localization on germ cell proliferation. **(F)** *(top)* Schematic of the CDC-20 region important for MAD-2 and APC/C-binding (KILR motif); the ΔPPP mutant selectively disrupts MAD-2 binding. *(bottom)* Yeast-two hybrid data showing the effect of the CDC-20 ΔPPP mutant on its interaction with MAD-2. **(G)** & **(H)** Checkpoint signaling *(G)* and germ cell proliferation *(H)* analysis in the indicated CDC-20 mutants. Dashed lines indicate average mitotic duration in bipolar (grey) and monopolar (red) controls. *(C,E,H)* Germ cell proliferation in 15 or more larvae was quantified at each time point; *(G) n* is number of embryos scored for mitotic duration. All error bars are 95% confidence intervals. **** represents $p<0.0001$ from Mann-Whitney tests. *See also* Figures S3 and S4.

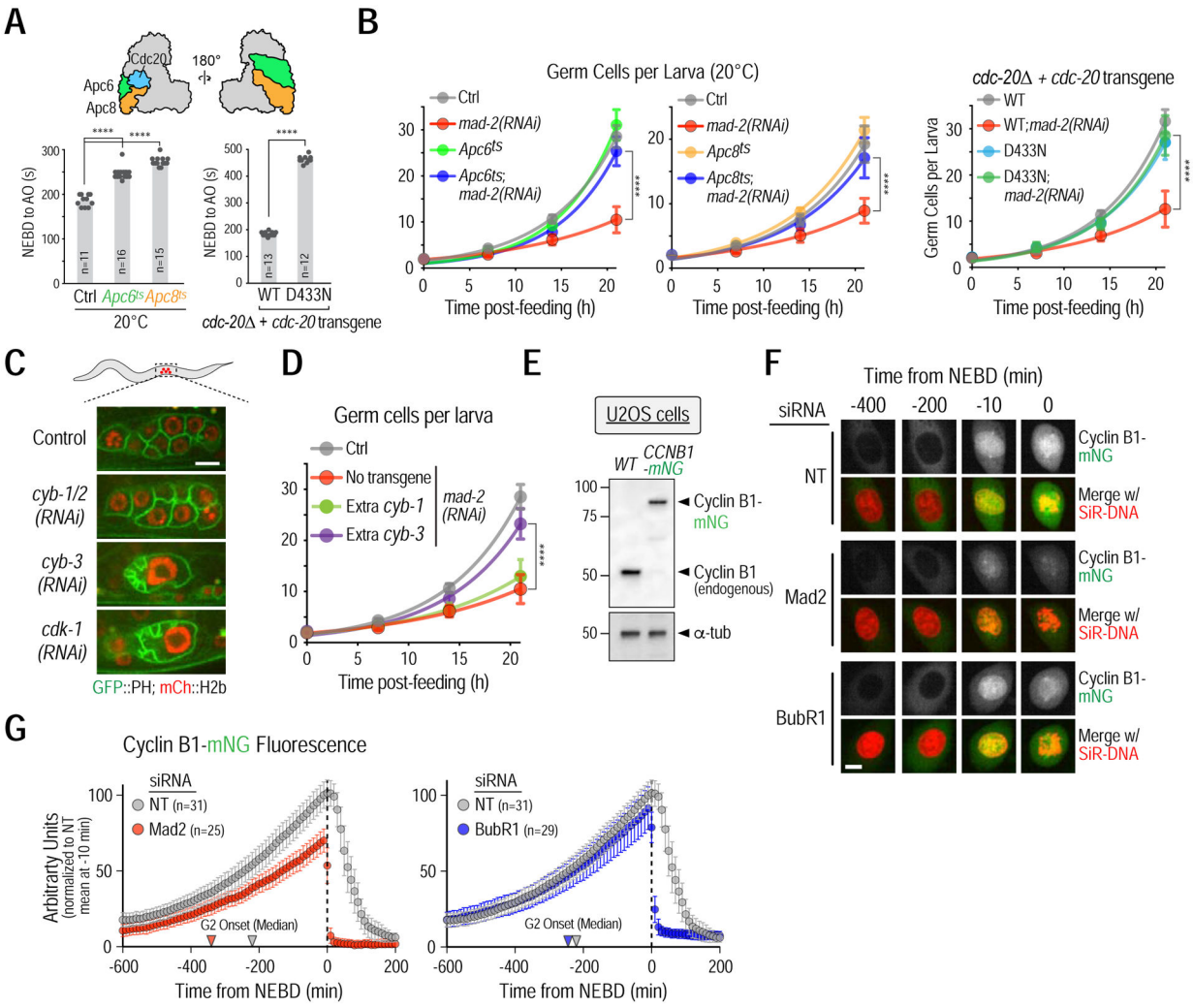

Figure 4. Mad2 inhibits APC/C^{Cdc20} to promote cyclin B accumulation.

(A) *(top)* Schematic highlighting the two structural APC/C subunits, Apc6 and Apc8, and the co-activator Cdc20, mutations in which were used to weaken APC/C^{CDC-20} activity. *(bottom)* NEBD-anaphase onset (AO) timing in one-cell embryos for the indicated conditions. **(B)** Germ cell proliferation analysis for the indicated conditions. **(C)** Effect of cyclin B isoform depletions, conducted by soaking larvae in dsRNA, on germ cell proliferation. Due to high sequence homology, the dsRNA used to deplete *cyb-1* is also expected to target *cyb-2*, hence it is refered to as *cyb-1/2*(*RNAi*). Bar, 5 μm. **(D)** Effect of doubling dosage of *cyb-1* or *cyb-3*, using functional single copy transgene insertions. Data for control and *mad-2*(*RNAi*) are the same as in panel B, left. **(E)** Cyclin B1 immunoblot of the indicated U2OS cell line extracts; α-tubulin serves as a loading control. **(F)** Representative images of Cyclin B1-mNeonGreen accumulation for the indicated conditions. Bar, 10 μm. **(G)** Quantification of total cyclin B1-mNeonGreen fluorescence over time. Arrowheads point to the median G2 onset time from Fig. 1G. All error bars are 95% confidence intervals. Asterisks represent p<0.0001 from Mann-Whitney tests; non-significant (n.s.) is p>0.05. *n* is the number of embryos or cells analyzed. >14 larvae were analyzed in germ cell proliferation assays. *See also* Figure S5.

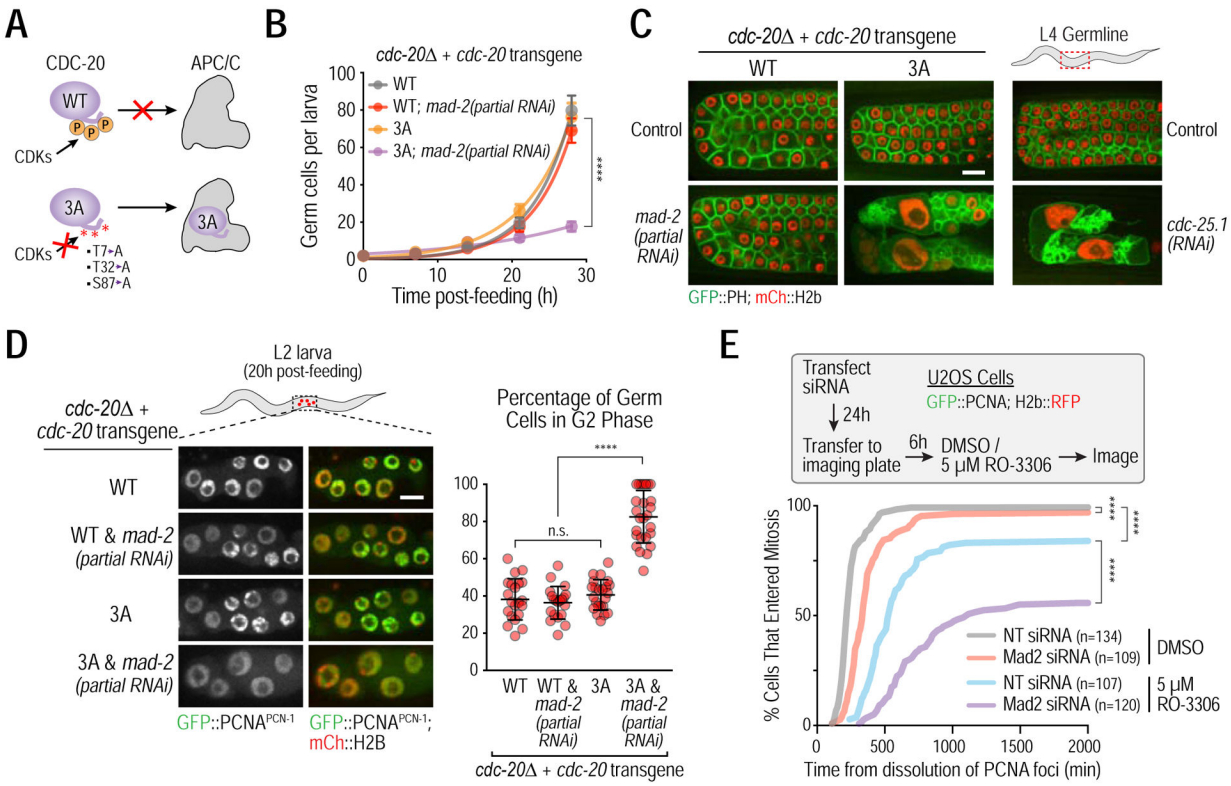

Figure 5. Cdc20 phosphorylation and Mad2 act in parallel to suppress APC/C^{Cdc20} activation in G2.

(A) Summary of the effect of Cdc20 phosphorylation by CDKs on its recruitment to the APC/C. 3A corresponds to a non-phosphorylatable CDC-20 mutant (Kim et al, 2017). **(B)** Germ cell proliferation analysis. As the CDC-20 phosphorylation mutant is synthetic lethal with spindle checkpoint inhibition in embryos, L1 larvae were subjected to post-hatching RNAi that results in partial MAD-2 inhibition. >15 larvae were quantified for each time point in germ cell proliferation analysis. Error bars are 95% confidence intervals. **(C)** Representative images of L4 larval stage germlines for the indicated conditions. Bar, 10 μm. **(D)** *(left)* Representative images and *(right)* plot of percentage of germ cells in G2, measured by GFP::PCNA^{PCN-1} imaging, 20h post-feeding of L1 larvae. Error bars are standard deviation. **(E)** *(top)* Experiment schematic and *(bottom)* plots of cumulative G2-to-M transition in U2OS cells as a function of time after PCNA foci dissolution for the indicated conditions. **** represents p<0.0001 from Mann-Whitney tests *(B,D)* or Kolmogorov-Smirnov test *(E)*; non-significant (n.s.) is p>0.05. *See also* Figure S6.

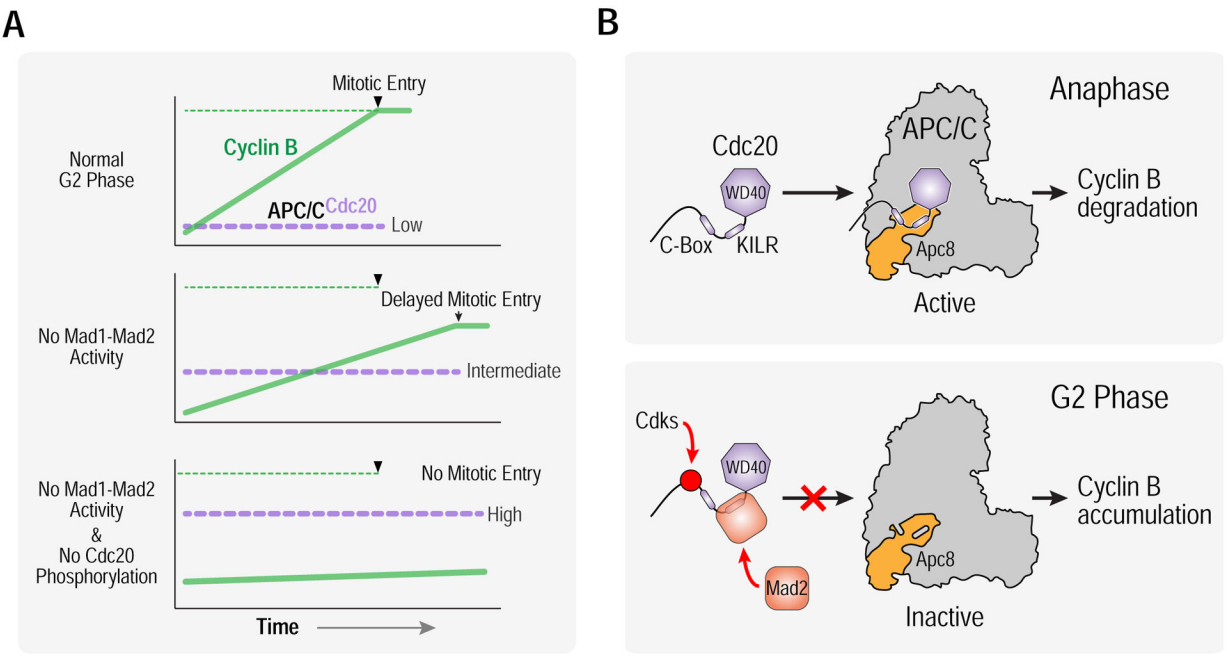

Figure 6. A dual mechanism targets APC/C binding motifs of Cdc20 to promote cyclin B accumulation and mitotic entry.

(A) Schematics highlighting normal G2 phase with cyclin B accumulation and transition into mitosis *(top)*, delayed cyclin B accumulation with an extended G2 phase and entry into mitosis at reduced cyclin B levels in the absence of Mad1/Mad2 activity *(middle)*, and a block to mitotic entry in the absence of both Mad1-Mad2 activity and Cdc20 phosphorylation by Cdks *(bottom)*. **(B)** *(top)* Cdc20 binds and activates APC/C to degrade cyclin B at anaphase onset, employing its C-box and KILR motif to bind to distinct sites on the Apc8 subunit. *(bottom)* To keep APC/C in check during G2 phase, Mad1-Mad2 catalyzes Mad2 binding to the KILR motif and Cdks phosphorylate resides adjacent to the C-box, thereby coordinately suppressing binding affinity of Cdc20 for the APC/C, preventing the formation of active APC/C^{Cdc20} complexes and allowing cyclin B to accumulate and trigger mitotic entry.

KEY RESOURCES TABLE

REAGENT or RESOURCE	SOURCE	IDENTIFIER
Antibodies		
Rabbit polyclonal anti MAD-2	(Essex et al., 2009)	OD72
Rabbit polyclonal anti MAD-3	This study	OD219-b
Rabbit polyclonal anti MAD-1 (aa 430–679)	(Moyle et al., 2014)	OD195-b
Rabbit polyclonal anti Cyclin B1	Cell Signaling	Cat #12231S; RRID AB_2783553
Rabbit polyclonal anti CDC-20 (aa 1–160)	(Kim et al., 2017)	OD220-b
Mouse monoclonal anti alpha-tubulin (clone DM1A)	Sigma-Aldrich	Cat #T9026; RRID AB_477593
Rabbit polyclonal anti-Mad2	Bethyl Laboratories	Cat #A300–301A; RRID AB_2281536
Sheep polyclonal anti-Mad2	(Tighe et al., 2008)	SM2.2
Rabbit polyclonal anti BubR1	(Kim et al., 2018)	N/A
Goat anti rabbit IgG, HRP-conjugated	Jackson Immunoresearch	Cat #111-035-003; RRID AB_2313567
Donkey anti mouse IgG, HRP-conjugated	Jackson Immunoresearch	Cat #715-035-150; RRID AB_2340770
Goat anti-mouse IgG, AP-conjugated	Promega	Cat #S372B; RRID AB_430871
Donkey anti-sheep IgG, HRP-conjugated	Thermo Fischer	Cat #A16041; RRID AB_2534715
Bacterial and Virus Strains		
Lentivirus: PGK promoter-Myc-Mad2-P2A-BSD	This study	N/A
Chemicals, Peptides, and Recombinant Proteins		
RO-3306	(Vassilev et al., 2006)	Sigma-Aldrich Cat #217699–5MG
Experimental Models: Cell Lines		
U2OS	ATCC	HTB-96
U2OS GFP-PCNA and H2b-RFP	(de Groot et al., 2015)	ODCL0033
U2OS GFP-PCNA and H2b-RFP; Myc-Mad2	This study	ODCL0094
U2OS CCNB1-mNeoNGreen	This study	ODCL0034
Experimental Models: Organisms/Strains		
C. elegans N2 Bristol	Caenorhabditis Genetics Center	N2
emb-27(g48ts)II	Caenorhabditis Genetics Center	GG48
mat-3(or344)III	Caenorhabditis Genetics Center	HY601
unc-119(ed3) ltIs38 [pAA1; pie-1/GFP::PH(PLC1delta1); cb-unc-119 (+)]III; ltIs37 [pAA64; pie-1/mCherry::his-58; cb-unc- 119 (+)]IV	(Green et al., 2011)	OD95
mdf-1(gk2)V/nT1(qIs51)(IV;V)	(Moyle et al., 2014)	OD738

REAGENT or RESOURCE	SOURCE	IDENTIFIER
ltSi219[pOD1248/pSW076; Pmex-5::GFP-PH(PLC1delta1)-operon-linker-mCherry-his-11; cb-unc-119(+)]I; unc-119(ed3)III	(Wang et al., 2015)	OD866
ltSi310[pOD1577/pMM7C; Pmdf-1::mdf-1::mdf-1 3'UTR; cb-unc-119(+)]II; unc-119(ed3)?III; mdf-1(gk2)V	(Moyle et al., 2014)	OD1051
ltSi608[pOD1583/pMM30; pmdf-1::GFP::mdf1::mdf-1 3'UTR; cb-unc-119(+)]II; unc-119(ed3)?III; mdf-1(gk2)V	(Moyle et al., 2014)	OD1208
ltSi608[pOD1583/pMM30; pmdf-1::GFP::mdf1::mdf-1 3'UTR; cb-unc-119(+)]II; unc-119(ed3)?III; ltIs37 [pAA64; pie-1/mCherry::his-58; unc-119 (+)] IV; mdf-1(gk2) V	(Moyle et al., 2014)	OD1209
unc-119(ed3)III; ltSi560[oxTi365; pPLG014; Pmex-5::GFP::his-11::tbb-2_3'UTR, tbg-1::gfp::tbb-2_3'UTR; cb-unc-119(+)]V	(Kim et al., 2015)	OD1702
emb-27(g48)II; unc-119(ed3)?III; ltSi560 [oxTi365; pPLG014; Pmex-5::GFP::his-11::tbb-2_3'UTR, tbg-1::gfp::tbb-2_3'UTR; cb-unc-119(+)]V	This study	OD1900
unc-119(ed3?) mat-3(or344)III; ltSi560 [oxTi365; pPLG014; Pmex-5::GFP::his-11::tbb-2_3'UTR, tbg-1::gfp::tbb-2_3'UTR; cb-unc-119(+)]V	(Kim et al., 2017)	OD2003
ltSi661[pPLG029; Pmdf-1::mdf-1(Q496A, I497A, F498A, H499A, M500A)::mdf-1 3'UTR; cb-unc-119(+)]II; unc-119(ed3)?III mdf-1(gk2) V/nT1(qIs51) (IV;V)	This study	OD2061
ltSi677 [pPLG034; Pmdf-1::GFP::mdf-1(delta 151–320)::mdf-1 3'UTR; cb-unc-119(+)]II; unc-119(ed3)?III; mdf-1(gk2)V/nT1(qIs51)(IV;V)	This study	OD2156
ltSi677 [pPLG034; Pmdf-1::GFP::mdf-1(delta 151–320)::mdf-1 3'UTR; cb-unc-119(+)]II; unc-119(ed3)?III; ltIs37 [pAA64; pie-1/mCherry::his-58; unc-119 (+)]IV; mdf-1(gk2)V/nT1(qIs51)(IV;V)	This study	OD2157
unc-119(ed3)?III; mdf-2(lt4::loxP::cb-unc-119(+)::loxP)IV	This study	OD2171
san-1(lt6::loxP::cb-unc-119(+)::loxP)I; unc-119(ed3)?III	This study	OD2172
unc-119(ed3)?III; mdf-2(lt4::loxP::cb-unc-119(+)::loxP)IV/nT1(qIs51)IV;V	This study	OD2174
san-1(lt6::loxP::cb-unc-119(+)::loxP)I; unc-119(ed3)?III/hT2[bli-4(e937) let-?(q782) qIs48](I;III)	This study	OD2175
unc-119(ed3?) mat-3(or344)III; mdf-1(gk2) ltSi560[oxTi365; pPLG014; Pmex-5::GFP::his-11::tbb-2_3'UTR, tbg-1::gfp::tbb-2_3'UTR; cb-unc-119(+)]V/ nT1[qIs51](IV;V)	This study	OD2236
ltSi587[pPLG024; Pmdf-2::mdf-2 delta intron 4::mdf-2 3'UTR; cb-unc-119(+)]II; unc-119(ed3)?III; mdf-2(lt4::loxP::cb-unc-119(+)::loxP)IV/nT1(qIs51)IV;V	This study	OD2300
ltSi808[pPLG044; Pmdf-2::mdf-2 delta intron 4 R133E, Q134A::mdf-2 3'UTR; cb-unc-119(+)]II; unc-119(ed3)?III; mdf-2(lt4::loxP::cb-unc-119(+)::loxP)IV/ nT1(qIs51)IV;V	This study	OD2453
ltSi310[pOD1577/pMM7C; Pmdf-1::mdf-1::mdf-1 3'UTR; cb-unc-119(+)]II; unc-119(ed3?) mat-3(or344)III; mdf-1(gk2) ltSi560[oxTi365; pPLG014; Pmex-5::GFP::his-11::tbb-2_3'UTR, tbg-1::gfp::tbb-2_3'UTR; cb-unc-119(+)]V/ nT1[qIs51](IV;V)	This study	OD2454
ltSi661[pPLG029; Pmdf-1::mdf-1(Q496A, I497A, F498A, H499A, M500A)::mdf-1 3'UTR; cb-unc-119(+)]II; unc-119(ed3?) mat-3(or344)III; mdf-1(gk2) ltSi560[oxTi365; pPLG014; Pmex-5::GFP::his-11::tbb-2_3'UTR, tbg-1::gfp::tbb-2_3'UTR; cb-unc-119(+)]V/nT1[qIs51](IV;V)	This study	OD2458
ltSi813[pPLG043; Pfzy-1::fzy-1 del 128–130::fzy-1 3'UTR; cb-unc-119(+)]I; fzy-1(lt20::loxP)/mIn1[mIs14 dpy-10(e128)]II; unc-119(ed3)?III	This study	OD2461
san-1(lt6::loxP::cb unc-119(+)::loxP)I; unc-119(ed3?) mat-3(or344)III; ltSi560[oxTi365; pPLG014; Pmex-5::GFP::his-11::tbb-2_3'UTR, tbg-1::gfp::tbb-2_3'UTR; cb-unc-119(+)]V	This study	OD2577
unc-119(ed3?) mat-3(or344)III; mdf-2(lt4::loxP::cb-unc-119(+)::loxP)IV; ltSi560 [oxTi365; pPLG014; Pmex-5::GFP::his-11::tbb-2_3'UTR, tbg-1::gfp::tbb-2_3'UTR; cb-unc-119(+)]V	This study	OD2579
ltSi822[pPLG051; Pfzy-1::fzy-1 A138V::fzy-1 3'UTR; cb-unc-119(+)]I; fzy-1(lt20::loxP)/mIn1[mIs14 dpy-10(e128)]II; unc-119(ed3)?III	This study	OD2580

REAGENT or RESOURCE	SOURCE	IDENTIFIER
ltSi813[pPLG043; Pfzy-1::fzy-1 del 128–130::fzy-1 3'UTR; cb-unc-119(+)]I;fzy-1(lt20::loxP)II; unc-119(ed3)?III; ltSi560 [oxTi365; pPLG014; Pmex-5::GFP::his-11::tbb-2_3'UTR, tbg-1::gfp::tbb-2_3'UTR; cb-unc-119(+)]V	This study	OD2583
ltSi813[pPLG043; Pfzy-1::fzy-1 del 128–130::fzy-1 3'UTR; cb-unc-119(+)]I;fzy-1(lt20::loxP)II; unc-119(ed3?) mat-3(or344)III; ltSi560 [oxTi365; pPLG014; Pmex-5::GFP::his-11::tbb-2_3'UTR, tbg-1::gfp::tbb-2_3'UTR; cb-unc-119(+)]V	This study	OD2584
ltSi822[pPLG051; Pfzy-1::fzy-1 A138V::fzy-1 3'UTR; cb-unc-119(+)]I; fzy-1(lt20::loxP)II; unc-119(ed3)?III; ltSi560 [oxTi365; pPLG014; Pmex-5::GFP::his-11::tbb-2_3'UTR, tbg-1::gfp::tbb-2_3'UTR; cb-unc-119(+)]V	This study	OD2585
ltSi822[pPLG051; Pfzy-1::fzy-1 A138V::fzy-1 3'UTR; cb-unc-119(+)]I; fzy-1(lt20::loxP)II; unc-119(ed3?) mat-3(or344)III; ltSi560 [oxTi365; pPLG014; Pmex-5::GFP::his-11::tbb-2_3'UTR, tbg-1::gfp::tbb-2_3'UTR; cb-unc-119(+)]V	(Kim et al., 2017)	OD2586
ltSi814[pPLG047; Pfzy-1::gfp::fzy-1::fzy-1 3'UTR; cb-unc-119(+)]I; unc-119(ed3)? III;; ltIs37 [pAA64; pie-1/mCherry::his-58; unc-119 (+)] IV	(Kim et al., 2017)	OD2591
ltSi825[pPLG052; Pmdf-2::mdf-2 delta intron 4::gfp::mdf-2 3'UTR; cb-unc-119(+)]II; unc-119(ed3)III?; mdf-2(lt4::loxP::cb-unc-119(+)::loxP)IV/nT1[qIs51](IV;V)	This study	OD2663
ltSi805[pPLG042; Pfzy-1::fzy-1::fzy-1 3'UTR; cb-unc-119(+)]I; fzy-1(lt20::loxP)/ mIn1[mIs14 dpy-10(e128)]II; unc-119(ed3)?III	(Kim et al., 2017)	OD2664
ltSi958[pPLG053; Pmdf-1::GFP::mdf-1 R518A, K519A, R520A, K521A::mdf-1 3'UTR; cb-unc-119(+)]II; unc-119(ed3)?III; mdf-1(gk2)V/nT1(qIs51)(IV;V)	This study	OD2685
ltSi958[pPLG053; Pmdf-1::GFP::mdf-1 R518A, K519A, R520A, K521A::mdf-1 3'UTR; cb-unc-119(+)]II; unc-119(ed3)?III; ltIs37[pAA64; pie-1/mCherry::his-58; unc-119 (+)]IV; mdf-1(gk2)V/nT1(qIs51)(IV;V)	This study	OD2686
ltSi959[pPLG054; Pmdf-1::GFP::mdf-1 d151–320 R518A, K519A, R520A, K521A::mdf-1 3'UTR; cb-unc-119(+)]II; unc-119(ed3)?III; mdf-1(gk2)V/nT1(qIs51) (IV;V)	This study	OD2687
ltSi959[pPLG054; Pmdf-1::GFP::mdf-1 d151–320 R518A, K519A, R520A, K521A::mdf-1 3'UTR; cb-unc-119(+)]II; unc-119(ed3)?III; ltIs37[pAA64; pie-1/ mCherry::his-58; unc-119 (+)]IV; mdf-1(gk2)V/nT1(qIs51)(IV;V)	This study	OD2688
ltSi805[pPLG042; Pfzy-1::fzy-1::fzy-1 3'UTR; cb-unc-119(+)]I; fzy-1(lt20::loxP)II; unc-119(ed3)?III; ltSi560 [oxTi365; pPLG014; Pmex-5::GFP::his-11::tbb-2_3'UTR, tbg-1::gfp::tbb-2_3'UTR; cb-unc-119(+)]V	(Kim et al., 2017)	OD2692
ltSi805[pPLG042; Pfzy-1::fzy-1::fzy-1 3'UTR; cb-unc-119(+)]I; fzy-1(lt20::loxP)II; unc-119(ed3?) mat-3(or344)III; ltSi560 [oxTi365; pPLG014; Pmex-5::GFP::his-11::tbb-2_3'UTR, tbg-1::gfp::tbb-2_3'UTR; cb-unc-119(+)]V	(Kim et al., 2017)	OD2693
emb-27(g48)II; unc-119(ed3)?III; mdf-2(lt4::loxP::cb-unc-119(+)::loxP)IV/nT1[qIs51] (IV;V)	This study	OD2832
mat-3(or344) unc-119(ed3)?III; mdf-2(lt4::loxP::cb-unc-119(+)::loxP)IV/nT1[qIs51] (IV;V)	This study	OD2835
mdf-1(lt39[gfp::tev::loxP::3xFlag::mdf-1])V	(Wang et al., 2017)	OD2906
unc-119(ed3?) mat-3(or344)III; ltIs37[pAA64; pie-1/mCherry::his-58; unc-119 (+)]IV	This study	OD2919
unc-119(ed3)?III; ltIs37[pAA64; pie-1/mCherry::his-58; unc-119 (+)]IV; mdf-1(lt39[gfp::tev::loxP::3xFlag::mdf-1])V	This study	OD2920
unc-119(ed3?) mat-3(or344)III; ltIs37[pAA64; pie-1/mCherry::his-58; unc-119 (+)]IV; mdf-1(lt39[gfp::tev::loxP::3xFlag::mdf-1])V	This study	OD3004
ltSi1066[pPLG187; Pmex-5::gfp::ph::tbb-2 3'-UTR::operon linker::mCherry::his-11::tbb-2 3'-UTR; cb-unc-119(+)]II; unc-119(ed3)III	This study	OD3328
ltSi1069[pPLG184; Pcyb-1::cyb-1::cyb-1 3'-UTR]II; unc-119(ed3)?III; mdf-2(lt4::loxP::cb-unc-119(+)::loxP)IV/nT1(qIs51)IV;V	This study	OD3336
ltSi1066[pPLG187; Pmex-5::gfp::ph::tbb-2 3'-UTR::operon linker::mCherry::his-11::tbb-2 3'-UTR; cb-unc-119(+)]II; unc-119(ed3)?III; mdf-2(lt4::loxP::cb-unc-119(+)::loxP)IV/nT1(qIs51)IV;V	This study	OD3338

REAGENT or RESOURCE	SOURCE	IDENTIFIER
san-1(lt6::loxP::cb-unc-119(+)::loxP)I; ltSi1066[pPLG187; Pmex-5::gfp::ph::tbb-2 3'-UTR::operon linker::mCherry::his-11::tbb-2 3'-UTR; cb-unc-119(+)]II; unc-119(ed3)?III	This study	OD3490
ltSi1066[pPLG187; Pmex-5::gfp::ph::tbb-2 3'-UTR::operon linker::mCherry::his-11::tbb-2 3'-UTR; cb-unc-119(+)]II; mat-3(or344) unc-119(ed3)?III	This study	OD3493
ltSi1093[pPLG207; Pmdf-1::mdf-1::mdf-1 3'UTR; cb-unc-119(+)]I; ltSi1066[pPLG187; Pmex-5::gfp::ph::tbb-2 3'-UTR::operon linker::mCherry::his-11::tbb-2 3'-UTR; cb-unc-119(+)]II; unc-119(ed3)?III; mdf-1(gk2) V/nT1(qIs51)(IV;V)	This study	OD3537
ltSi1096[pPLG208; Pmdf-1::mdf-1(Q496A, I497A, F498A, H499A, M500A)::mdf-1 3'UTR; cb-unc-119(+)]I; ltSi1066[pPLG187; Pmex-5::gfp::ph::tbb-2 3'-UTR::operon linker::mCherry::his-11::tbb-2 3'-UTR; cb-unc-119(+)]II; unc-119(ed3)?III; mdf-1(gk2) V/nT1(qIs51)(IV;V)	This study	OD3538
ltSi1112[pPLG217; Pmex-5::gfp::pcn-1::tbb-2 3'-UTR::operon linker::mCherry::his-11::tbb-2 3'-UTR; cb-unc-119(+)]II; unc-119(ed3)III	This study	OD3549
ltSi805[pPLG042; Pfzy-1::fzy-1::fzy-1 3'UTR; cb-unc-119(+)]I; fzy-1(lt20::loxP) ltSi1066[pPLG187; Pmex-5::gfp::ph::tbb-2 3'-UTR::operon linker::mCherry::his-11::tbb-2 3'-UTR; cb-unc-119(+)]II/mIn1[mIs14 dpy-10(e128)]II; unc-119(ed3)?III	This study	OD3554
mdf-2(lt104[mdf-2::gfp::tev::loxP::3xFlag])IV	This study	OD3637
unc-119(ed3?)III; mdf-2(lt104[mdf-2::gfp::tev::loxP::3xFlag]) ltIs37[pAA64; pie-1/mCherry::his-58; unc-119 (+)]IV	This study	OD3655
cyb-3(lt110)V/nT1[qIs51](IV;V).	This study	OD3737
cyb-1(gk35) IV/nT1[qIs51](IV;V)	This study	OD3739
unc-119(ed3?) mat-3(or344)III; ltIs37[pAA64; pie-1/mCherry::his-58; unc-119 (+)] mdf-2(lt105[mdf-2::gfp::tev::loxP::3xFlag])IV	This study	OD3740
ltSi1112[pPLG217; Pmex-5::gfp::pcn-1::tbb-2 3'-UTR::operon linker::mCherry::his-11::tbb-2 3'-UTR; cb-unc-119(+)]II; cdk-1(ne2257) unc-119(ed3)?III	This study	OD3830
ltSi1069[pPLG184; Pcyb-1::cyb-1::cyb-1 3'-UTR]II; unc-119(ed3)?III; cyb-1(gk35)IV/nT1[qIs51](IV;V)	This study	OD3837
ltSi1138[pPLG240; Pcyb-3::cyb-3::cyb-3 3'UTR; cb-unc-119(+)]I; cyb-3(lt110)V/nT1[qIs51](IV;V)	This study	OD3838
ltSi1138[pPLG240; Pcyb-3::cyb-3::cyb-3 3'UTR; cb-unc-119(+)]I; unc-119(ed3)?III; mdf-2(lt4::loxP::cb-unc-119(+)::loxP)IV/nT1(qIs51)IV;V	This study	OD3842
cyb-2.2(tm1969)I; cyb-2.1(tm2027)IV	This study	OD3844
ltSi1167[oxTi185; pPLG187; Pmex-5::gfp::ph::tbb-2 3'-UTR::operon linker::mCherry::his-11::tbb-2 3'-UTR; cb-unc-119(+)]I; unc-119(ed3)III	This study	OD3908
ltSi1167[oxTi185; pPLG187; Pmex-5::gfp::ph::tbb-2 3'-UTR::operon linker::mCherry::his-11::tbb-2 3'-UTR; cb-unc-119(+)] ltSi1138[pPLG240; Pcyb-3::cyb-3::cyb-3 3'UTR; cb-unc-119(+)]I; unc-119(ed3)?III	This study	OD3910
ltSi1167[oxTi185; pPLG187; Pmex-5::gfp::ph::tbb-2 3'-UTR::operon linker::mCherry::his-11::tbb-2 3'-UTR; cb-unc-119(+)]I; ltSi1069[pPLG184; Pcyb-1::cyb-1::cyb-1 3'-UTR]II; unc-119(ed3)?III	This study	OD3911
cyb-1(lt125[cyb-1::LAP::mNeonGreen::loxP::3xFlag])IV	This study	OD3913
ltSi1167[oxTi185; pPLG187; Pmex-5::gfp::ph::tbb-2 3'-UTR::operon linker::mCherry::his-11::tbb-2 3'-UTR; cb-unc-119(+)]I; emb-27(g48ts)II; unc-119(ed3)?III	This study	OD3942
ltSi310[pOD1577/pMM7C; Pmdf-1::mdf-1::mdf-1 3'UTR; cb-unc-119(+)]II; unc-119(ed3)?III; mdf-2(lt104[mdf-2::gfp::tev::loxP::3xFlag]) ltIs37[pAA64; pie-1/mCherry::his-58; unc-119(+)]IV; mdf-1(gk2)V	This study	OD4050

REAGENT or RESOURCE	SOURCE	IDENTIFIER
ltSi976[pPLG063; Pmdf-1::mdf-1 delta 151–320::mdf-1 3'UTR; cb-unc-119(+)]II; unc-119(ed3)?III; mdf-2(lt104[mdf-2::gfp::tev::loxP::3xFlag]) ltIs37[pAA64; pie-1/mCherry::his-58; unc-119(+)]IV; mdf-1(gk2) V	This study	OD4051
ltSi587[pPLG024; Pmdf-2::mdf-2 delta intron 4::mdf-2 3'UTR; cb-unc-119(+)]II; unc-119(ed3)? mat-3(or344)III; mdf-2(lt4::loxP::cb-unc-119(+)::loxP)IV; ltSi560[oxTi365; pPLG014; Pmex-5::GFP::his-11::tbb-2_3'UTR, tbg-1::gfp::tbb-2_3'UTR; cb-unc-119(+)]V	This study	OD4058
ltSi808[pPLG044; Pmdf-2::mdf-2 delta intron 4 R133E, Q134A::mdf-2 3'UTR; cb-unc-119(+)]II; unc-119(ed3)? mat-3(or344)III; mdf-2(lt4::loxP::cb-unc-119(+)::loxP)IV; ltSi560[oxTi365; pPLG014; Pmex-5::GFP::his-11::tbb-2_3'UTR, tbg-1::gfp::tbb-2_3'UTR; cb-unc-119(+)]V	This study	OD4059
ltSi822[pPLG051; Pfzy-1::fzy-1 A138V::fzy-1 3'UTR; cb-unc-119(+)]I; fzy-1(lt20::loxP) ltSi1066[pPLG187; Pmex-5::gfp::ph::tbb-2 3'-UTR::operon linker::mCherry::his-11::tbb-2 3'-UTR; cb-unc-119(+)]II/mIn1[mIs14 dpy-10(e128)]II; unc-119(ed3)?III	This study	OD4060
ltSi1195[pPLG256; Pfzy-1::fzy-1 D433N::fzy-1 3'UTR; cb-unc-119(+)]I; fzy-1(lt20::loxP) ltSi1066[pPLG187; Pmex-5::gfp::ph::tbb-2 3'-UTR::operon linker::mCherry::his-11::tbb-2 3'-UTR; cb-unc-119(+)]II; unc-119(ed3)?III	This study	OD4062
ltSi1195[pPLG256; Pfzy-1::fzy-1 D433N::fzy-1 3'UTR; cb-unc-119(+)]I; fzy-1(lt20::loxP)II; unc-119(ed3)?III; ltSi560 [oxTi365; pPLG014; Pmex-5::GFP::his-11::tbb-2_3'UTR, tbg-1::gfp::tbb-2_3'UTR; cb-unc-119(+)]V	This study	OD4063
ltSi1200[pPLG262; Pmdf-1::GFP::mdf-1(Q496A, I497A, F498A, H499A, M500A)::mdf-1 3'UTR; cb-unc-119(+)]II; unc-119(ed3)?III; ltIs37[pAA64; pie-1/mCherry::his-58; unc-119 (+)]IV; mdf-1(gk2)V/nT1(qIs51)(IV;V)	This study	OD4071
ltSi1088[oxTi185; pMO005; Pmex-5::mCherry::ph::tbb-2 3'-UTR::operon linker::mCherry::his-11::tbb-2 3'-UTR]I; ltSi608[pOD1583/pMM30; pmdf-1::GFP::mdf1::mdf-1 3'UTR; cb-unc-119(+)]II; unc-119(ed3)?III; mdf-1(gk2) V	This study	OD4083
ltSi1088[oxTi185; pMO005; Pmex-5::mCherry::ph::tbb-2 3'-UTR::operon linker::mCherry::his-11::tbb-2 3'-UTR]I; ltSi677 [pPLG034; Pmdf-1::GFP::mdf-1(delta 151–320)::mdf-1 3'UTR; cb-unc-119(+)]II; unc-119(ed3)? III; unc-119 (+)]IV; mdf-1(gk2)V	This study	OD4084
ltSi1088[oxTi185; pMO005; Pmex-5::mCherry::ph::tbb-2 3'-UTR::operon linker::mCherry::his-11::tbb-2 3'-UTR]I; ltSi958[pPLG053; Pmdf-1::GFP::mdf-1 R518A, K519A, R520A, K521A::mdf-1 3'UTR; cb-unc-119(+)]II; unc-119 (+)]IV; mdf-1(gk2)V	This study	OD4085
ltSi1088[oxTi185; pMO005; Pmex-5::mCherry::ph::tbb-2 3'-UTR::operon linker::mCherry::his-11::tbb-2 3'-UTR]I; ltSi959[pPLG054; Pmdf-1::GFP::mdf-1 d151–320 R518A, K519A, R520A, K521A::mdf-1 3'UTR; cb-unc-119(+)]II; unc-119(ed3)?III; mdf-1(gk2)V	This study	OD4086
unc-119(ed3)?III; cyb-1(lt125[cyb-1::LAP::mNeonGreen::loxP::3xFlag]) ltIs37[pAA64; pie-1/mCHERRY::his-58; unc-119 (+)]IV	This study	OD4100
unc-119(ed3)?III; ltIs37[pAA64; pie-1/mCHERRY::his-58; unc-119 (+)]IV; cyb-3(lt135[mNeonGreen::tev::loxP::3xFlag::cyb-3])V	This study	OD4102
ltSi813[pPLG043; Pfzy-1::fzy-1 del 128–130::fzy-1 3'UTR; cb-unc-119(+)]I; fzy-1(lt20::loxP) ltSi1066[pPLG187; Pmex-5::gfp::ph::tbb-2 3'-UTR::operon linker::mCherry::his-11::tbb-2 3'-UTR; cb-unc-119(+)]II/mIn1[mIs14 dpy-10(e128)]II; unc-119(ed3)?III	This study	OD4139
ltSi965[pPLG058; Pfzy-1::fzy-1 T7A, T32A, S87A::fzy-1 3'UTR; cb-unc-119(+)]I; fzy-1(lt20::loxP) ltSi1066[pPLG187; Pmex-5::gfp::ph::tbb-2 3'-UTR::operon linker::mCherry::his-11::tbb-2 3'-UTR; cb-unc-119(+)]II; unc-119(ed3)?III	This study	OD4192
ltSi805[pPLG042; Pfzy-1::fzy-1::fzy-1 3'UTR; cb-unc-119(+)]I; fzy-1(lt20::loxP); ltSi1112[pPLG217; Pmex-5::gfp::pcn-1::tbb-2 3'-UTR::operon linker::mCherry::his-11::tbb-2 3'-UTR; cb-unc-119(+)]II; unc-119(ed3?)III	This study	OD4225
ltSi965[pPLG058; Pfzy-1::fzy-1 T7A, T32A, S87A::fzy-1 3'UTR; cb-unc-119(+)]I; fzy-1(lt20::loxP); ltSi1112[pPLG217; Pmex-5::gfp::pcn-1::tbb-2 3'-UTR::operon linker::mCherry::his-11::tbb-2 3'-UTR; cb-unc-119(+)]]II; unc-119(ed3?)III	This study	OD4226
Oligonucleotides		

REAGENT or RESOURCE	**SOURCE**	**IDENTIFIER**
CRISPR/Cas9 targeting sequences, see Table S1	This paper	N/A
Primers for dsRNA production, see Table S2	This paper	N/A
ON-TARGETplus Non-targeting Pool	Dharmacon	Cat # L-015475-00-0005
Mad2 siRNA #1, CCUAUUGAAUCAGUUUCCAAUUU	(Ye et al., 2017)	N/A
Mad2 siRNA #2, CAGUAUAGGUAGGGAGAUAUU	(Ye et al., 2017)	N/A
ON-TARGETplus Human BUB1B siRNA - SMARTpool	Dharmacon	Cat # L-004101-00-0005
Software and Algorithms		
Fiji	(Schindelin et al., 2012)	RRID: SCR_002285
Prism	Graphpad	RRID: SCR_002798